The HST Key Project on the Extragalactic Distance Scale

XX. The Discovery of Cepheids in the Virgo Cluster Galaxy NGC 4548 [1]

John A. Graham[2], Laura Ferrarese[3,4], Wendy L. Freedman[5], Robert C. Kennicutt, Jr.[6], Jeremy R. Mould[7], Abhijit Saha[8], Peter B. Stetson[9], Barry F. Madore[10], Fabio Bresolin [6,11], Holland C. Ford[12], Brad K. Gibson[7], Mingsheng Han[13], John G. Hoessel[13], John Huchra[14], Shaun M. Hughes[15], Garth D. Illingworth[16], Lucas Macri[14] Daniel D. Kelson[6,2], Randy Phelps[5], Shoko Sakai[8], & N.A. Silbermann[10] Anne Turner[6]

Received _____; accepted _____

---

[1]Based on observations with the NASA/ESA *Hubble Space Telescope*, obtained at the Space Telescope Science Institute, which is operated by AURA, Inc. under NASA Contract NO. NAS5-26555.

[2]Department of Terrestrial Magnetism, Carnegie Institution of Washington, Washington DC 20015, USA

[3]Hubble Fellow

[4]California Institute of Technology, Pasadena CA 91125, USA

[5]Carnegie Observatories, Pasadena CA 91101, USA

[6]Steward Observatories, University of Arizona, Tucson AZ 85721, USA

[7]Mount Stromlo and Siding Spring Observatories, Institute of Advanced Studies, ANU, ACT 2611, Australia

[8]Kitt Peak National Observatory, NOAO, Tucson AZ 85726, USA

[9]Dominion Astrophysical Observatory, Victoria, British Columbia V8X 4M6, Canada

[10]NASA/IPAC, California Institute of Technology, Pasadena CA 91125, USA

[11]European Southern Observatory, Garching b. München, Germany

[12]Johns Hopkins University and Space Telescope Science Institute, Baltimore MD 21218, USA

[13]University of Wisconsin, Madison WI 53706, USA

[14]Harvard Smithsonian Center for Astrophysics, Cambridge MA 02138 USA

[15]Royal Greenwich Observatory, Cambridge CB3 OHA, UK

[16]Lick Observatory, University of California, Santa Cruz CA 95064 USA

ABSTRACT

We report on the discovery and properties of Cepheid variable stars in the barred spiral galaxy NGC 4548 which is a member of the Virgo cluster of galaxies. This is one of the galaxies being observed as part of the Hubble Space Telescope (HST) Key Project on the Extragalactic Distance Scale which aims to determine the Hubble Constant to 10% accuracy. Our analysis is based on observations made with the Wide Field and Planetary Camera 2 during 1996 and 1997. We identify 26 probable Cepheids with periods between 16 and 38 days. They were observed over 13 epochs with the F555W filter and 8 epochs with the F814W filter. The HST F555W and F814W data have been transformed to the Johnson V and Cousins I magnitude systems respectively. Photometry has principally been carried out using the DAOPHOT/ALLFRAME package. A comparison is made with parallel measurements using the DoPHOT package.

Apparent period-luminosity functions for V and I have been constructed. Assuming values of $\mu_0 = 18.50 \pm 0.10$ mag and $E(B-V) = 0.10$ mag for the distance modulus and reddening of the Large Magellanic Cloud, a true distance modulus of 31.03 ± 0.26 mag is derived corresponding to a distance of 16.1 ± 2.0 Mpc. Cepheid distances of other spiral galaxies within the Virgo Cluster core are discussed. With the exception of NGC 4639, which seems to be on the far side of the cluster, the average distance of 6 spiral galaxies is found to be 16.0 Mpc with an uncertainty which depends mainly on the base calibration.

Subject headings: galaxies: individual(NGC 4548) — galaxies: distances — galaxies: clusters(Virgo) — stars: Cepheids

1. Introduction

The ultimate aim of the Hubble Space Telescope (HST) Key Project on the extragalactic distance scale is to enable the Hubble constant to be determined within 10% (Kennicutt, Freedman & Mould 1995). The essence of this HST program is to determine Cepheid distances via the period-luminosity (PL) relation to 18 galaxies with redshifts out to about 1500 km sec^{-1}. The Virgo Cluster galaxies are playing a significant part in providing the calibration for the secondary distance indicators which bridge local flow perturbations and enlarge the volume over which a global Hubble constant can be derived. As well as NGC 4548, the subject of this paper, two other Virgo galaxies are included in the HST program. They are NGC 4321 (Ferrarese et al. (1996) and NGC 4535 (Macri et al. 1998). We are also re-reducing HST data obtained by others for three additional galaxies, NGC 4496A, NGC4536 and NGC4639.

We chose NGC 4548 as a well resolved spiral galaxy which has a high probability of membership in the Virgo Cluster (de Vaucouleurs & de Vaucouleurs 1973, Binggeli, Tammann & Sandage 1987). It is centered at $\alpha_{2000}=12^h\ 35^m\ 26^s.3$, $\delta_{2000}=+14°\ 29'\ 49''$, 2.4° NE of the giant elliptical galaxy Messier 87. The heliocentric velocity is 475 km sec^{-1} (Rubin, Waterman & Kenney 1999) which is small compared to that of the Virgo Cluster as a whole but is in no way exceptional. The galaxy type is SBb(rs)I-II (Sandage & Tammann 1981) and SBb(rs) (de Vaucouleurs et al. 1991). The nucleus shows low-ionization emission (Ho, Filipppenko & Sargent 1995). Rubin et al. estimate an inclination of 37°. Ground based images are published in the Carnegie Atlas of Galaxies (Sandage & Bedke 1994). The galaxy appears similar to NGC 3351 which was the subject of one of our earlier papers (Graham et al. 1997). Van den Bergh (1975) refers to it as "a fine example of an anemic spiral". NGC 4548 can probably be identified with Messier 91 although some historical uncertainty exists (Mallas & Kreimer 1978).

2. Observations and Data Reduction

Our observing strategy is discussed in detail in previous papers of this series (e.g. Ferrarese et al. 1996, 1998) and we refer to these for more complete descriptions. Here we discuss only those issues which relate directly to NGC 4548. The HST observations began on 1996 April 16 using the Wide Field and Planetary Camera 2 (WFPC2). For the principal data set, a total of 40 V images at 12 epochs, spaced over a 60 day interval, was accumulated using the F555W filter. Within this same interval 24 additional images were obtained at 8 of the 12 epochs with the F814W filter to measure I magnitudes. All observations were carried out at the same telescope pointing and roll angle. For this series of observations, a displacement of a few pixels was introduced between each epoch of observation to improve the sampling capability and the removal of bad pixel elements for each frame. An additional follow-up pair of images, with the F555W filter only, was obtained during a revisit on 1997 May 5, 324 days after the last observation of the main data set. This pair was used to improve the precision of the Cepheid periods.

The region we have observed in NGC 4548 is shown in Figure 1 which is taken from an image obtained with the 1.2 m telescope at the F.W. Whipple Observatory of the Smithsonian Institution. The PC chip covers the smallest field. We refer to this as chip 1. The three WFC chips cover the 3 larger fields. We will refer to these as chips 2, 3 and 4 as encountered when one moves anti-clockwise from the PC field in the figure. The summary of observations and exposure times is given in Table 1. The sampling strategy has been discussed by Freedman et al. (1994). The actual observations followed very closely our requested sampling sequence. Figure 2 illustrates the probability that a variable with period P is detected given the temporal sampling on the assumption that all initial phases are equally likely. The calculation excluded the revisit epoch because these observations were not used for the variable star search. Incompleteness due to magnitude selection effects is

not taken into account. This becomes severe for faint stars because of the large measuring errors in the magnitudes. From the slope of the period-luminosity (PL) relation and the incompleteness at fainter magnitudes, Cepheid variable stars are unlikely to be discovered at periods less than 15 days in this galaxy.

Routine calibration via the standard pipeline maintained by the Space Telescope Science Institute (STScI) has been carried out as described in previous papers of this series. All exposures were taken at the low CCD operating temperature of −88° so that the hot pixel problem and the "charge transfer" photometry gradient (Holtzman et al. 1995a, Hill et al. 1998) were minimized. Although this latter gradient has now been more precisely specified (Whitmore & Heyer 1997), no additional corrections have been made at this time.

3. Photometric Reduction

Photometric analysis of HST frames was carried out independently by Graham using DAOPHOT and ALLFRAME (Stetson 1994) and by Ferrarese using DoPHOT (Schechter, Mateo, & Saha 1993). As pointed out in earlier papers (e.g. Ferrarese et al. 1996), the philosophy behind the two program packages is quite different. Thus there is a useful check on the results for random systematic errors which might otherwise go unnoticed if a single program is used. For example, noise events cause different responses in the two programs and the methods for determining sky background are not the same.

Procedures described in the earlier papers were again followed in the ALLFRAME measurements. Small corrections are necessary to bring the photometry to the standard systems used by others with the HST (Hill et al. 1998). These include the aperture corrections which were computed to bring the ALLFRAME magnitudes to the equivalent of aperture photometry with an aperture diameter of 0.5 arcsec (Holtzman et al. 1995b).

Approximately 25 isolated stars were selected from the ALLFRAME photometry lists to determine, with the DAOGROW routine, image growth curves showing magnitude as a function of aperture. The initial solutions, particularly those for the PC (chip 1) and WF2 (chip 2) frames were ill-defined and did not lead to credible results. This was largely because of the lack of stars of sufficient brightness with low measuring errors. New solutions were therefore made for all chips by averaging image growth curves computed for other galaxies of the Key Project along with some star cluster and parallel field data. The resulting aperture corrections are given in Table 2. The values agree well with those derived earlier for chips 3 and 4 and are more precise than those first determined for chips 1 and 2.

The DoPHOT photometry was performed using a variant of the DoPHOT package (Schechter et al. 1993, Saha et al. 1994) which was developed especially to deal with the photometry of undersampled images such as those obtained with the HST. Discussion of this application of DoPHOT to photometry of HST images can be found in Saha et al. (1996a), Ferrarese et al. (1996, 1998), and Hill et al. (1998).

A color correction was also applied. We again used the following relations suggested by Holtzman et al. (1995b) to obtain V and I magnitudes on the Johnson and Cousins systems respectively.

$$V = \mathrm{F555W} - 0.052(V\text{–}I) + 0.027(V\text{–}I)^2$$

$$I = \mathrm{F814W} - 0.063(V\text{–}I) + 0.025(V\text{–}I)^2$$

Except for very red stars, the color correction is small, no more than a few hundredths of a magnitude. We have again included the correction of 0.05 mag to our long exposure frames as discussed in Hill et al. (1998).

The bright stars used to determine the ALLFRAME aperture corrections are convenient reference stars for present and future comparisons of our photometry and we list them in Table 3 along with x, y positions, right ascension and declination with the mean ALLFRAME and DoPHOT magnitudes converted to the standard VI system. In the identification column, the first figure refers to the chip number, the second to the number of the reference star on that chip. Identical procedures were followed in processing the photometry of the Cepheid variable stars (section 5). In every case the x, y coordinates refer to the first frames at the first epoch of the set. The equatorial coordinates are based on the *nominal* pointing of the Space Telescope and are calculated using the *metric* program in the IRAF/STSDAS software package. The actual pointings of the telescope agree with the planned ones to within 0.6 arcsec, well within the overall uncertainty ($\approx$ 1 arcsec) of the coordinate system as a whole.

4. Comparison between ALLFRAME and DoPHOT Magnitudes

The independent data reductions using ALLFRAME and DoPHOT provide an external test of the point spread function (PSF) fitting accuracy in these crowded and complicated star fields. A detailed discussion and comparison will be presented in a future paper (Stetson et al. in preparation). Here we summarize the results of our comparisons for NGC 4548. We first compared the photometry for the isolated bright stars (Table 3) and then performed the same comparison for the Cepheid variable stars of our final sample (Table 5). The differences are plotted in Figure 3 and listed in Table 4. The agreement is not uniformly good, illustrating the difficulty in analysing fields as distant and as crowded as

those found in NGC 4548. Chip-to-chip differences as large as 0.14 mag are found. The average difference for all Cepheids is small in V (+0.03 mag) but large in I (+0.09 mag) and this directly impacts on our distance determinations (section 7). When separated according to different chip numbers, it can be seen in Table 4 that the large differences in the Cepheid photometry are associated with large (but generally more precisely determined) differences in the photometry of the bright stars. For both groups of stars, the largest differences are found for chip 3 and chip 4 which (cf. Figure 1) include the brightest background contribution from the NGC 4548 itself. Crowding of faint, partially resolved stars must complicate the definition of a background "sky measurement" in these fields. In addition there is the problem of separating close, and more frequently redder companion stars. Tests conducted with artificial stars have shown that ALLFRAME may not resolve close companions stars as well as DoPHOT although both procedures are likely to be deficient in fields as crowded as these. The same tests point to errors in determining the aperture corrections as the most likely source of the discrepancy. With the few bright, isolated stars available, their determination remains a formidable task. However, the use of two separate photometry packages does allow us to quantify external uncertainties of this type.

5. Variable Star Search

5.1. DAOPHOT/ALLFRAME Data Set

Two methods have been used to search the DAOPHOT/ALLFRAME data set. They complement each other by emphasizing in turn the tasks of detecting variability and searching for periodicity. The first method is described by Welch & Stetson (1993). It depends on the simple concept that, while photometric measuring errors have a random distribution with time, residuals due to intrinsic variability are likely to be strongly correlated. The method works especially well with the HST data sets in which observations

are grouped for random event (cosmic ray) removal. A variability index is computed for each of the stars measured by ALLFRAME. A filter is incorporated into the program to remove the large differences which may be introduced by isolated erroneous magnitudes. This filter also serves to remove epochs for which ALLFRAME finds itself unable to measure a sensible magnitude and outputs instead an unrealistically large one. A lower limit on the the correlation index needs to be specified in order to limit the suspect list to those stars which are likely variable. With star lists often containing several thousand stars, random positive correlations naturally occur. The resulting list is then sorted in decreasing value of the index. The true variable stars are usually found at the top of this list. Occasionally, a bad pixel measurement will produce a single epoch magnitude which will distort the index and give an erroneous detection. Such cases are easily spotted by inspection.

Another powerful method of Cepheid detection is to attempt to fit a period for the sequence of measured magnitudes. For this, a version of the Lafler-Kinman (1965) technique as formulated by Stellingwerf (1978) has been used. The "phase dispersion minimum" (*pdm*) program takes the data set and, with a trial period, computes phases. The magnitude list is reordered in phase and the program computes a difference sum for a succession of trial periods. The spacing of the trial periods depends on the time base of the data set. When there is a real periodic variation, the difference sum becomes small as the best period is approached. Some caution has to be used to eliminate spurious periods, which, for example, may represent two, and not just a single cycle. The method is most effective at finding periods between 0.25 and 1.0 times the time base of the data set. For shorter periods, it gets confused by photometric errors and will contribute spurious periods. Experience has shown that the *pdm* method is more sensitive to large errors in the photometry (e.g. from random events on the chip) than the correlated residuals method. The initial search and period search were derived only with the main data set of V magnitudes from the 12 epochs covering a time base of 60 days. Periods around the reported *pdm* period were then

examined and the best period selected by taking into account the observational uncertainty and phase value of individual magnitudes in the sequence. The best period was usually within a day of the reported *pdm* period. The mean magnitude of the revisit observation, made 324 days later, was then incorporated into the data set and, again with the recognition of the measuring uncertainties, was used to refine the period of the variable star. Final periods are listed in Table 5 with estimates of their uncertainties.

5.2. DoPHOT Data Set

The search for variable stars was performed on the V band images following the procedure described by Saha & Hoessel (1990). We required that a star be detected at at least 10 of the 12 epochs in order to be checked for variability. We also excluded all stars in crowded regions by rejecting candidates with a companion contributing more than 50% of the total light in a two pixel radius. A detailed discussion of search procedure can be found in Ferrarese et al. (1996). A star meeting the above constraints was flagged as a variable if $\chi^2_r \geq 8$ or $\Lambda \geq 3$ where χ^2_r and Λ are as used in Saha & Hoessel (1990).

Several spurious variables were registered by this procedure as a consequence of non-gaussian sources of error and various anomalies of the images (e.g. residual cosmic ray events) along with the crowding referred to earlier. Each potentially variable star was visually inspected by blinking several of the individual frames against each other. With the DoPHOT data set, the best period for each variable was selected by phasing the data for all periods between 3 and 100 days in incremental steps of 0.1 days. Although in most cases the final period adopted corresponds to a minimum value of the phase dispersion, in a few cases here also, an obvious improvement of the light curve was obtained for a slightly different period.

5.3. Search Results

Our aim is to obtain a sample of Cepheid variable stars with properties similar to those known in the Galaxy and the Large Magellanic Cloud (LMC). Thus the prime criterion for accepting a star as such in NGC 4548 is the appearance of the light curve relating magnitude to phase-wrapped epoch. Numerical parameters, such as those based on correlated residuals or phase dispersion minima are invaluable for discovery but quantitatively are susceptible to random events and photometric errors. They are not helpful in distinguishing long period variables, eclipsing stars and novae, for example, from Cepheids. More sophisticated routines for doing just this are currently being tested at the Dominion Astrophysical Observatory by Stetson (1996). Typical Cepheid light curves are well-known from the LMC sample (e.g. Wayman, Stifft, & Butler 1984). They are sometimes sinusoidal but more often show a rise in brightness more rapid than the decline. In some senses, discrimination by light curve-shape parameters alone is a more quantitative procedure but decisions about the critical values used for the parameters are themselves based on personal experience. Thus the decision process is only moved back one step. Inclusion of Cepheid variables pulsating in the first overtone (Böhm-Vitense 1988) is a concern only for stars with periods less than 10 days. While Population II W Virginis stars might be expected in a spiral galaxy with a type as early as that of NGC 4548, reference to published PL relations (Nemec & Lutz 1993) shows that even the longest period examples of these stars would be much fainter than our detection limit.

After engaging in separate searches with ALLFRAME and DoPHOT, we compared candidate lists and examined in detail those stars flagged in only one search. We found this double search reassuring. Most variables (28) indeed were found independently in both data sets. In 7 cases with only a single discovery, the explanation lay in the different treatment of random events by the two different procedures. A more thorough analysis of

the effect of samples found separately by ALLFRAME and DoPHOT is given by Ferrarese et al. (1996). There it is shown that the resulting distance moduli are not sensitive to small changes in the selection criteria for variables or the source of the sample. Artificial stars simulations on crowded fields (Ferrarese et al. 1998), show that incompleteness biases are negligible (less than 10% of stars are lost) at V magnitudes brighter than 26.5 mag. $V = 27.5$ mag or fainter stars need to be reached before more than 50% of the sample is lost. These numbers refer to a complete list of stars, and grossly overestimate the number of stars lost in *uncrowded* parts of the field, where almost all of the Cepheids used in fitting the PL relation are found. The tests by Ferrarese et al. predict that a significant loss of Cepheids due to magnitude incompleteness is present in the NGC 4548 field only at periods shorter than 20 days.

Our final list of 26 Cepheid variables is given in Table 5. The ALLFRAME and DoPHOT periods were reviewed by Graham and a consensus value determined which is entered into Table 5 with the appropriate uncertainty. Coordinates based on WFPC2 measurements and the nominal position of the telescope are given. Finding charts are provided in Figures 4 and 5. The photometry is given in Tables 6 and 7. Table 8 contains a list of variable stars which are either not Cepheids or are suspected Cepheids which were excluded from the main list because of poor photometry. Finding charts for these stars are given in Figure 6.

6. Light Curves and Mean Magnitudes

The light curves, based on the V magnitudes phased to the periods in Table 5, are reproduced in Figure 7. They are arranged in order of decreasing period and are lined up so that phase = 1.0 corresponds to maximum brightness. They are folded over two cycles to highlight their morphology. The adopted period is shown in each panel. A characteristic

error reported by ALLFRAME for the magnitudes in each set is shown in the lower left corner of each panel. A perusal of the panels in Figure 7 confirms that they are typical of curves expected from normal Cepheid variable stars with the rise to maximum being faster than the decline to minimum.

Mean V and I magnitudes are routinely computed in two different ways; as intensity averaged magnitudes $< V >_i$, $< I >_i$ and as phase weighted magnitudes $< V >_{ph}$, $< I >_{ph}$ (see Saha & Hoessel 1990b). For variable stars with uniformly sampled light curves, these coincide but whenever the phase coverage of the light curve is not uniform, higher weighting of the less common phase points provides a more accurate estimate of the mean magnitude than a simple intensity average. Both are listed in Table 9 for each Cepheid variable star along with the period. In the NGC 4548 data set, I magnitude coverage (8 epochs) is almost as good as that for V (12 epochs) and, for this galaxy, we did not see the need for computing $< I >_{\Delta I}$ which result from mapping the I magnitudes onto the V magnitude light curve (see Freedman 1988, Graham et al. 1997). A comparison between intensity averaged magnitudes and phase weighted magnitudes for V and I confirms that the phase sampling is not a problem. The mean $< V >_i - < V >_{ph} = -0.016 \pm 0.009$ mag with an average numerical difference per star of 0.04 mag. The mean $< I >_i - < I >_{ph} = -0.003 \pm 0.011$ mag with an average numerical difference per star again of 0.04 mag.

An I, V–I color-magnitude diagram for all stars is shown as Figure 8. Cepheids are marked as filled circles, other stars as points. The Cepheids lie in a band bounded by V–I = 0.6 and 1.4 mag. The color magnitude diagram for all stars that we measured illustrates mainly the color characteristics of the faint magnitude cut-off. It is similar to that of NGC 3351 (Graham et al. 1997) if allowance is made for the greater distance of NGC 4548.

7. Period-Luminosity Relations and the Distance to NGC 4548

Following other papers in this series, the apparent V and I distance moduli to NGC 4548 are to be based on the DAOPHOT/ALLFRAME data set. Again, the V and I PL relations found by Madore and Freedman (1991) are used. These depend on LMC Cepheid data scaled to a true modulus of 18.5 mag corrected for an average line-of-sight E($B-V$) reddening of 0.10 mag [E($V-I$) = 0.13 mag]. They are:

$$< V > = -2.76 \log \mathrm{P} - 1.40$$

$$< I > = -3.06 \log \mathrm{P} - 1.81$$

Note that these calibration relations include overtone pulsating variable stars. They would be different, and more physically correct, if these short period stars had been excluded. However, we have chosen to adopt this calibration as it is for all Key Project galaxies. This assures homogeneity and does not introduce biases in the derived distances since the shape of the PL relations are kept fixed thoughout. Only the zero point is allowed to vary, not the slope. Larger samples of LMC Cepheids are becoming available and it is forseeable that an improved, more precise PL calibration will be available in the near future. Indeed, we plan to revise all of the derived distances when this calibration is redone.

Phase averaged magnitudes are used in our fitting procedure. The V and I PL plots are shown for the ALLFRAME data in Figures 9 and 10. The solid lines represent the best unweighted fit. The dashed lines, drawn at ± 0.54 mag in Figure 9 and at ± 0.36 mag in

Figure 10 reflect the finite width of the Cepheid instability strip. The functional relations are

$$< V > = -2.76 \log \mathrm{P} + 29.91$$

$$< I > = -3.06 \log \mathrm{P} + 29.39$$

These lead to V and I moduli of 31.31 $\pm$ 0.07 and 31.20 $\pm$ 0.05 mag respectively with $\mathrm{E}(V-I) = 0.12 \pm 0.03$ mag for the NGC 4548 Cepheids. Using the procedures described in earlier papers of this series, the apparent moduli are related through a dust extinction law. An extinction law consistent with that of Cardelli, Clayton & Mathis (1989) with A_B: A_V: A_I = 1.3: 1.0: 0.6 and $\mathrm{R}_V = \mathrm{A}_V$ / $\mathrm{E}(V-I)$ of 2.45 which takes into account the actual effective wavelength of the Cousins I band is used to derive a true modulus of 31.03 $\pm$ 0.05 mag corresponding to a distance of 16.1 $\pm$ 0.4 Mpc. This assumes $\mathrm{R}_V = \mathrm{A}_V$ / $\mathrm{E}(B-V) = 3.3$. The corresponding relations for the DoPHOT data are:

$$< V > = -2.76 \log \mathrm{P} + 29.87$$

$$< I > = -3.06 \log \mathrm{P} + 29.26$$

These lead to V and I moduli of 31.27 $\pm$ 0.07 and 31.10 $\pm$ 0.06 mag respectively with $E(V-I) = 0.17 \pm 0.03$ mag and a true modulus of 30.86 $\pm$ 0.07 mag. The errors as before are internal errors and for the individual apparent moduli are correlated. Thus the true modulus has a smaller error than one would expect if the V and I moduli were completely independent. The DoPHOT true modulus corresponds to 14.9 $\pm$ 0.4 Mpc. The difference between the two distances draws attention to the disturbing sensitivity to the reddening determinations based on two color photometry alone. They are a direct consequence of the mean difference in the DoPHOT and ALLFRAME photometric scales in the I band (section 3). DoPHOT, it will be recalled, determines I magnitudes for Cepheids which are on the average 0.09 mag brighter than from ALLFRAME although the mean differences in V are close to zero. The different internal reddening implied levers the change in the internal absorption estimate which is responsible for the different distances. While the photometry is capable of some improvement, we feel strongly that the only way to firmly address this problem is to push our photometry further to the infrared which has distinct advantages once the period of the Cepheid is known (McGonegal et al. 1982). At present, we feel we can do no better than to propose the ALLFRAME values which have the smaller scatter and to embrace the difference in our overall error assesment.

The effect of metallicity on Cepheid distances remains a controversial issue which will probably not be finally resolved until infrared data becomes available. The recent work by Kennicutt et al. (1998) found only a weak dependence of the inferred distance modulus on metal abundance, and its impact seems very contained. We have decided not to attempt a correction for this at the present time. As in previous papers, an error budget has been drawn up for our new distance and is shown in Table 10. An additional uncertainty in our determination is the LMC distance modulus ($\pm$0.10) and incorporating this in quadrature with the above, we find the mean modulus 31.04 $\pm$ 0.26 mag corresponds to a distance of 16.1 $\pm$ 2.0 Mpc.

8. Cepheid Distances for Galaxies in the Virgo Cluster

As Aaronson & Mould (1986) made clear, Cepheid variable stars are widely regarded as the best primary indicators of distances to external galaxies. The basic physics is well understood. The dispersion in absolute magnitude is small and quantifiable. Cepheids can be measured in enough galaxies for the calibration to be checked and rechecked and its sensitivity to parameters such as metallicity and interstellar absorption evaluated. However, it has only been with the HST that routine observation of the Cepheid variables in many galaxies has become possible. Only fragmentary observations, for example, could be made of Virgo Cluster galaxies from the ground (e.g. NGC 4571, Pierce et al. (1994)). Yet, the Virgo Cluster contains so many galaxies of such diverse types that, regardless of the uncertain dynamics and the probable extension in depth, it is an essential staging post for the calibration of those secondary distance indicators which can extend our measuring capability far beyond.

Over the last few years, several new distances to Virgo cluster galaxies have been published based on Cepheid variable star observations with the HST and the consequent PL relations. These are listed in Table 11 along with the Revised Shapley Ames type (Sandage and Tammann 1981) and the angular distance of each galaxy from the luminosity weighted cluster center at $12^h\ 27.8^m$ $+12°\ 56'$ (Huchra 1985). Although NGC 4496A and NGC 4536 are more than 6° from this center (the strict defintion of the Virgo Cluster core), they are still within the cluster as defined by Binggeli, Tammann and Sandage (1987). The Pierce et al. ground based distance for NGC 4571 is also included in the Table even though it is based on only 3 Cepheids.

Distances based on Cepheid absolute magnitudes are no more accurate than the period-luminosity relations on which they are based. All the galaxy distances listed in Table 11 rest on the same LMC Cepheid calibration published by Madore & Freedman (1991) and

will change together, should that calibration be improved. Following the publication by Feast & Catchpole (1997) of the first results of *Hipparcos* parallaxes for Galactic Cepheids, Madore & Freedman (1998) have re-examined their earlier calibration to see whether modifications are appropriate at this stage. They use the new individual distances to calibrate the PL relation at six wavelengths ($BVIJHK$). Current parallax errors dominate the uncertainty and they conclude that the above LMC modulus is still the most consistent one to use.

Most of the galaxies in Table 11 have distances very close to our mean value for NGC 4548, the main exception being NGC 4639 which, according to both Saha et al. (1997) and Gibson et al. (1998), has a distance several Mpc beyond the other Virgo galaxies in Table 11. Yet, with a heliocentric velocity of 975 km sec^{-1} (Rubin, Waterman & Kenney 1999), there seems no doubt of its membership of the Virgo cluster. There is some supporting evidence for the greater distance from the Tully-Fisher data (Pierce & Tully 1988) which shows that NGC 4639 has a significantly larger (0.6 mag) distance modulus than NGC 4548. The mean distance for the 7 galaxies in Table 11 is 17.5 Mpc. Excluding NGC 4639, the mean is 16.0 Mpc. The small scatter of the Cepheid distances is remarkable and suggests that the spirals are defining a centroid distance close to 16 Mpc. Some caution is in order. When looking for galaxies which resolve well, there may have been a tendency to select those on the near side of the Virgo Cluster. However, we note that in the recent paper by Böhringer et al. (1997), it is argued that NGC 4548 must indeed be close to the center of the cluster because it shows signs of being stripped of its H I. Its low velocity would in fact suggest that it is on the far side rather than the near side of the core. Ideally, more Cepheid distances for other Virgo spirals galaxies would clarify the situation but it may be many years before these become available. In the interim, the compactness of the core might best be evaluated by studying the relative dispersion of secondary distance indicators in individual galaxies. For example, Jacoby, Ciardullo & Ford (1990) noted from their study

of planetary nebulae around 6 other galaxies of earlier Hubble type that the dispersion in distance among galaxies within the Virgo cluster core was also small, probably less than 1.0 Mpc. Their mean distance was 14.7 Mpc, not significantly different from the mean Cepheid distance when uncertainties in calibration zero-points are taken into account.

We would again like to thank Doug Van Orsow, the program coordinator for this Key Project as well as the rest of the STScI and NASA support staff. Financial support for this work was provided by NASA through grant GO-2227-87A from STScI. LF ackowledges support by NASA through Hubble Fellowship grant HF-01081.01-96A awarded by the Space Telescope Science Institute. PBS and SMGH are grateful to NATO for travel assistance via a Collaborative Research Grant (960178).

Table 1. Log of Observations

Obs. Date	JD (mid-exp)	Exposure Time (sec)	Filter
16/04/96	2450189.820	1200	F555W
16/04/96	2450189.836	1200	F555W
16/04/96	2450189.886	1200	F555W
16/04/96	2450189.904	1300	F814W
16/04/96	2450189.954	1300	F814W
16/04/96	2450189.970	1300	F814W
24/04/96	2450197.998	1100	F555W
24/04/96	2450198.013	1100	F555W
24/04/96	2450198.062	1100	F555W
24/04/96	2450198.078	1100	F555W
24/04/96	2450198.130	1200	F814W
24/04/96	2450198.142	1200	F814W
24/04/96	2450198.013	1200	F814W
05/05/96	2450208.920	1200	F555W
05/05/96	2450208.936	1200	F555W
05/05/96	2450208.985	1200	F555W
05/05/96	2450209.002	1300	F814W
05/05/96	2450208.053	1300	F814W
05/05/96	2450208.070	1300	F814W
07/05/96	2450211.065	1200	F555W
07/05/96	2450211.065	1200	F555W
07/05/96	2450211.081	1200	F555W
07/05/96	2450211.130	1300	F555W

Table 1—Continued

Obs. Date	JD (mid-exp)	Exposure Time (sec)	Filter
07/05/96	2450211.147	1300	F555W
10/05/96	2450213.947	1200	F555W
10/05/96	2450213.963	1200	F555W
10/05/96	2450214.011	1200	F555W
10/05/96	2450214.029	1300	F814W
10/05/96	2450214.079	1300	F814W
10/05/96	2450214.095	1300	F814W
14/05/96	2450217.900	1200	F555W
14/05/96	2450217.916	1200	F555W
14/05/96	2450217.965	1300	F555W
14/05/96	2450217.982	1300	F555W
17/05/96	2450221.050	1200	F555W
17/05/96	2450221.066	1200	F555W
17/05/96	2450221.115	1200	F555W
17/05/96	2450221.132	1300	F814W
17/05/96	2450221.181	1300	F814W
17/05/96	2450221.199	1300	F814W
21/05/96	2450225.272	1200	F555W
21/05/96	2450225.288	1200	F555W
21/05/96	2450225.337	1300	F555W
21/05/96	2450225.354	1300	F555W
26/05/96	2450229.895	1200	F555W
26/05/96	2450229.911	1200	F555W

Table 1—Continued

Obs. Date	JD (mid-exp)	Exposure Time (sec)	Filter
26/05/96	2450229.959	1200	F555W
26/05/96	2450229.976	1300	F814W
26/05/96	2450230.027	1300	F814W
26/05/96	2450230.044	1300	F814W
31/05/96	2450235.122	1200	F555W
31/05/96	2450235.138	1200	F555W
31/05/96	2450235.186	1300	F555W
31/05/96	2450235.203	1300	F555W
07/06/96	2450241.960	1200	F555W
07/06/96	2450241.975	1200	F555W
07/06/96	2450242.023	1200	F555W
07/06/96	2450242.040	1300	F814W
07/06/96	2450242.090	1300	F814W
07/06/96	2450242.107	1300	F814W
15/06/96	2540249.736	1200	F555W
15/06/96	2540249.752	1200	F555W
15/06/96	2540249.800	1200	F555W
15/06/96	2540249.816	1300	F814W
15/06/96	2540249.866	1300	F814W
15/06/96	2540249.883	1300	F814W
05/05/97	2540574.239	2300	F555W
05/05/97	2540574.305	2600	F555W

Table 2. ALLFRAME Aperture Corrections

Chip	Correction	s.e.
	(a) F555W (V)	
1	−0.17	0.01
2	−0.04	0.01
3	−0.01	0.01
4	+0.00	0.01
	(b) F814W (I)	
1	−0.17	0.01
2	+0.00	0.01
3	+0.01	0.01
4	+0.01	0.01

Table 3. Positions and Magnitudes of Bright Stars

Star	x	y	R.A.(2000) h m s	Dec.(2000) ° ′ ″	V^{ALL}	I^{ALL}	V^{DoP}	I^{DoP}
1- 1	264.70	279.27	12 35 29.76	14 28 21.77	24.44	24.46	24.51	24.53
1- 2	243.63	327.97	12 35 29.73	14 28 19.41	23.49	23.22	23.60	23.32
1- 3	493.97	383.56	12 35 30.53	14 28 19.33	23.48	23.09	23.60	23.19
1- 4	506.68	539.21	12 35 30.67	14 28 12.54	27.03	23.87	27.14	24.02
2- 1	232.91	125.31	12 35 28.54	14 28 09.87	24.20	24.32	24.23	24.27
2- 2	511.05	133.28	12 35 28.90	14 27 42.77	24.48	24.22	24.47	24.16
2- 3	374.74	156.48	12 35 28.55	14 27 55.48	24.43	24.13	24.40	24.09
2- 4	543.40	198.06	12 35 28.52	14 27 38.22	26.80	24.09	26.71	24.00
2- 5	300.36	270.59	12 35 27.67	14 28 00.22	26.14	23.80	26.09	23.70
2- 6	294.16	393.16	12 35 26.85	14 27 58.16	24.18	23.90	24.23	23.87
2- 7	304.62	394.10	12 35 26.86	14 27 57.12	24.75	23.76	24.71	23.70
2- 8	263.74	428.99	12 35 26.56	14 28 00.32	23.64	23.46	23.70	23.40
3- 1	550.00	149.82	12 35 25.33	14 28 28.82	23.31	23.07	23.21	22.93
3- 2	565.53	242.54	12 35 25.09	14 28 37.46	23.44	22.38	23.40	22.27
3- 3	533.72	243.60	12 35 25.30	14 28 38.23	23.45	22.92	23.38	22.78
3- 4	731.42	245.20	12 35 23.98	14 28 34.27	23.91	23.69	23.81	23.56
3- 5	760.02	293.73	12 35 23.72	14 28 38.37	25.27	23.93	25.14	23.79
3- 6	360.20	364.21	12 35 26.28	14 28 53.60	22.99	22.92	22.97	22.78
3- 7	404.33	498.48	12 35 25.79	14 29 05.71	23.69	23.35	23.67	23.19
4- 1	281.70	125.74	12 35 29.13	14 28 54.41	23.52	22.60	23.54	22.54
4- 2	88.31	261.54	12 35 30.31	14 28 38.38	23.29	23.03	23.25	22.94
4- 3	453.94	383.97	12 35 30.62	14 29 16.37	23.41	23.31	23.55	23.22
4- 4	633.13	415.02	12 35 30.58	14 29 34.42	24.76	22.69	24.69	22.59
4- 5	233.22	436.05	12 35 31.28	14 28 55.94	24.32	22.76	24.36	22.67
4- 6	153.55	446.14	12 35 31.46	14 28 48.40	26.88	24.13	26.88	24.08
4- 7	207.41	491.78	12 35 31.69	14 28 54.56	23.33	23.03	23.36	22.94
4- 8	108.29	493.04	12 35 31.83	14 28 44.99	23.54	23.25	23.55	23.19
4- 9	360.70	523.57	12 35 31.69	14 29 10.12	23.06	22.36	23.13	22.29
4-10	736.20	589.20	12 35 31.60	14 29 47.84	23.40	23.24	23.44	23.19
4-11	718.24	647.92	12 35 32.02	14 29 47.26	23.96	23.56	23.94	23.44

Table 4. DAOPHOT/ALLFRAME minus DoPHOT Photometry

Chip	No. Stars	$\overline{\Delta V}$	No. Stars	$\overline{\Delta I}$
		(a) Bright Stars		
1	4	-0.10 ± 0.01	4	-0.11 ± 0.03
2	8	$+0.01 \pm 0.02$	8	$+0.06 \pm 0.01$
3	7	$+0.07 \pm 0.02$	7	$+0.14 \pm 0.01$
4	11	-0.02 ± 0.02	11	$+0.08 \pm 0.01$
		(b) Cepheids		
1	5	-0.08 ± 0.06	4	-0.06 ± 0.03
2	5	$+0.06 \pm 0.03$	4	$+0.10 \pm 0.06$
3	8	$+0.13 \pm 0.02$	8	$+0.13 \pm 0.07$
4	8	-0.02 ± 0.01	8	$+0.13 \pm 0.03$

Table 5. Positions and Periods for Cepheid Variables

Star	Chip	x	y	R.A.(2000) h m s	Dec.(2000) ° ′ ″	P (days)
C01	3	768.83	239.70	12 35 23.74	14 28 32.97	33.2 ±0.1
C02	3	752.23	165.29	12 35 23.96	14 28 26.15	18.4 ±0.1
C03	3	694.22	262.29	12 35 24.20	14 28 36.69	24.8 ±0.1
C04	2	99.62	664.26	12 35 24.75	14 28 11.02	29.5 ±0.2
C05	2	199.52	587.17	12 35 25.41	14 28 03.09	24.2 ±0.2
C06	2	212.35	553.53	12 35 25.65	14 28 02.59	19.1 ±0.5
C07	3	331.86	359.76	12 35 26.48	14 28 53.77	17.1 ±0.1
C08	2	340.89	447.83	12 35 26.55	14 27 52.43	31.0±0.2
C09	3	164.31	514.70	12 35 27.37	14 29 12.35	38.2±0.2
C10	3	179.16	311.60	12 35 27.57	14 28 52.34	18.8±0.1
C11	3	79.84	400.76	12 35 28.10	14 29 03.08	23.7±0.1
C12	3	51.98	337.40	12 35 28.38	14 28 57.53	29.4±0.1
C13	2	317.56	158.00	12 35 28.45	14 28 00.98	18.0±0.2
C14	4	440.26	275.85	12 35 29.91	14 29 12.85	31.0±0.1
C15	4	393.44	279.03	12 35 30.00	14 29 08.37	17.5±0.2
C16	1	347.54	553.91	12 35 30.20	14 28 10.36	29.2±0.2
C17	1	357.13	559.09	12 35 30.23	14 28 10.23	17.5±0.2
C18	1	529.87	394.30	12 35 30.65	14 28 19.20	35.0±0.2
C19	1	541.11	727.13	12 35 30.90	14 28 04.57	16.5±0.1
C20	1	558.87	666.46	12 35 30.92	14 28 07.41	17.5±0.1
C21	4	275.85	425.79	12 35 31.15	14 28 59.87	28.2±0.1
C22	4	386.47	478.48	12 35 31.35	14 29 11.71	16.9±0.1
C23	4	346.62	492.30	12 35 31.50	14 29 08.11	21.2±0.1
C24	4	599.65	603.94	12 35 31.89	14 29 34.96	20.2±0.1
C25	4	273.89	730.72	12 35 33.19	14 29 05.89	23.3±0.1
C26	4	267.47	771.26	12 35 33.47	14 29 06.09	17.0±0.1

Table 6. ALLFRAME V Photometry for NGC 4548 Cepheids

JD	$V \pm \sigma_V$	$V \pm \sigma_V$	$V \pm \sigma_V$	$V \pm \sigma_V$	$V \pm \sigma_V$	$V \pm \sigma_V$
2450000+	C1	C2	C3	C4	C5	C6
189.847	25.91 ± 0.11	26.24 ± 0.14	26.60 ± 0.16	25.36 ± 0.08	26.05 ± 0.13	26.39 ± 0.16
198.024	26.44 ± 0.16	26.74 ± 0.19	26.07 ± 0.13	25.48 ± 0.10	26.66 ± 0.25	26.63 ± 0.16
208.947	26.69 ± 0.18	26.04 ± 0.11	26.06 ± 0.09	25.48 ± 0.08	26.04 ± 0.09	26.28 ± 0.14
211.106	26.17 ± 0.13	26.18 ± 0.16	26.24 ± 0.12	25.26 ± 0.06	25.97 ± 0.10	26.67 ± 0.16
213.640	26.02 ± 0.12	26.46 ± 0.15	26.48 ± 0.12	25.24 ± 0.08	26.23 ± 0.13	26.78 ± 0.19
217.940	25.74 ± 0.09	26.62 ± 0.15	26.47 ± 0.16	25.37 ± 0.08	26.37 ± 0.14	27.06 ± 0.24
221.077	25.92 ± 0.11	27.56 ± 0.36	26.23 ± 0.05	25.51 ± 0.07	26.32 ± 0.11	27.18 ± 0.44
225.313	26.12 ± 0.13	26.94 ± 0.13	25.64 ± 0.15	25.76 ± 0.09	27.16 ± 0.23	25.87 ± 0.09
229.922	26.32 ± 0.13	26.03 ± 0.13	25.72 ± 0.09	25.80 ± 0.10	26.82 ± 0.19	26.30 ± 0.13
235.162	26.77 ± 0.18	26.42 ± 0.13	26.13 ± 0.13	25.96 ± 0.13	25.98 ± 0.10	26.80 ± 0.18
241.986	26.54 ± 0.15	26.57 ± 0.21	26.69 ± 0.19	25.17 ± 0.07	26.33 ± 0.18	27.14 ± 0.28
249.763	25.82 ± 0.10	26.09 ± 0.11	25.77 ± 0.08	25.48 ± 0.07	26.67 ± 0.16	26.55 ± 0.18
574.203	26.51 ± 0.18	27.06 ± 0.21	25.67 ± 0.07	25.47 ± 0.13	25.95 ± 0.27	26.40 ± 0.10
2450000+	C7	C8	C9	C10	C11	C12
189.847	25.86 ± 0.11	26.49 ± 0.13	25.41 ± 0.08	26.58 ± 0.20	26.50 ± 0.18	25.40 ± 0.09
198.024	26.90 ± 0.18	26.40 ± 0.12	26.09 ± 0.13	25.91 ± 0.13	26.29 ± 0.16	25.65 ± 0.12
208.947	25.90 ± 0.11	26.08 ± 0.13	26.33 ± 0.19	26.25 ± 0.38	26.56 ± 0.16	26.22 ± 0.16
211.106	26.34 ± 0.30	26.37 ± 0.24	26.48 ± 0.17	25.56 ± 0.09	26.63 ± 0.17	26.34 ± 0.14
213.640	26.66 ± 0.15	26.30 ± 0.26	26.45 ± 0.25	25.66 ± 0.10	26.84 ± 0.26	26.21 ± 0.16
217.940	26.72 ± 0.25	26.33 ± 0.11	26.45 ± 0.18	26.18 ± 0.18	25.87 ± 0.11	25.55 ± 0.09
221.077	26.45 ± 0.17	26.48 ± 0.11	26.90 ± 0.11	26.61 ± 0.16	26.08 ± 0.13	25.18 ± 0.08
225.313	26.04 ± 0.12	26.41 ± 0.13	25.43 ± 0.09	26.89 ± 0.20	26.60 ± 0.15	25.51 ± 0.09
229.922	26.47 ± 0.15	26.38 ± 0.12	25.71 ± 0.10	25.42 ± 0.09	26.66 ± 0.18	25.84 ± 0.11
235.162	27.03 ± 0.18	25.60 ± 0.07	25.89 ± 0.11	25.79 ± 0.10	26.59 ± 0.25	26.20 ± 0.15
241.986	25.98 ± 0.11	26.07 ± 0.10	26.22 ± 0.15	26.75 ± 0.19	26.88 ± 0.12	26.42 ± 0.23
249.763	26.76 ± 0.24	26.42 ± 0.11	26.49 ± 0.22	25.32 ± 0.08	26.27 ± 0.16	25.17 ± 0.09
574.203	26.86 ± 0.15	26.03 ± 0.09	25.62 ± 0.08	25.93 ± 0.07	25.89 ± 0.13	25.29 ± 0.12
2450000+	C13	C14	C15	C16	C17	C18
189.847	26.71 ± 0.18	26.01 ± 0.12	25.54 ± 0.08	25.97 ± 0.11	27.03 ± 0.29	26.16 ± 0.14
198.024	26.76 ± 0.25	25.97 ± 0.12	26.62 ± 0.18	26.40 ± 0.21	25.94 ± 0.11	26.82 ± 0.16
208.947	26.77 ± 0.20	25.35 ± 0.08	25.87 ± 0.12	25.82 ± 0.12	27.02 ± 0.25	27.30 ± 0.22
211.106	26.95 ± 0.22	25.50 ± 0.09	26.04 ± 0.13	25.88 ± 0.10	27.00 ± 0.21	27.47 ± 0.23
213.640	26.88 ± 0.21	25.47 ± 0.08	26.56 ± 0.14	25.96 ± 0.11	26.08 ± 0.10	26.41 ± 0.34
217.940	26.78 ± 0.20	25.84 ± 0.10	26.93 ± 0.25	25.92 ± 0.09	26.48 ± 0.11	25.96 ± 0.09

Table 6—Continued

JD	$V \pm \sigma_V$	$V \pm \sigma_V$	$V \pm \sigma_V$	$V \pm \sigma_V$	$V \pm \sigma_V$	$V \pm \sigma_V$
221.077	26.22 ± 0.14	26.03 ± 0.12	26.80 ± 0.18	25.95 ± 0.09	27.07 ± 0.20	26.04 ± 0.08
225.313	26.39 ± 0.17	26.12 ± 0.12	25.82 ± 0.09	26.20 ± 0.11	27.38 ± 0.24	26.38 ± 0.13
229.922	27.19 ± 0.28	25.58 ± 0.08	26.10 ± 0.10	26.53 ± 0.16	27.00 ± 0.18	26.76 ± 0.15
235.162	26.87 ± 0.17	25.03 ± 0.07	26.89 ± 0.21	26.06 ± 0.11	26.43 ± 0.14	26.92 ± 0.22
241.986	26.58 ± 0.15	25.36 ± 0.10	25.58 ± 0.08	25.97 ± 0.10	27.13 ± 0.24	26.92 ± 0.27
249.763	27.27 ± 0.30	25.72 ± 0.08	26.42 ± 0.24	25.93 ± 0.11	26.11 ± 0.12	26.49 ± 0.17
574.203	27.18 ± 0.19	25.11 ± 0.06	25.86 ± 0.08	26.12 ± 0.09	26.83 ± 0.29	26.11 ± 0.11
2450000+	C19	C20	C21	C22	C23	C24
189.847	26.92 ± 0.23	25.85 ± 0.12	25.42 ± 0.07	26.76 ± 0.23	26.34 ± 0.14	26.16 ± 0.14
198.024	26.87 ± 0.24	27.00 ± 0.20	25.92 ± 0.12	25.80 ± 0.11	25.49 ± 0.09	26.82 ± 0.16
208.947	26.74 ± 0.20	26.09 ± 0.12	26.32 ± 0.17	26.43 ± 0.19	25.80 ± 0.10	27.30 ± 0.22
211.106	26.97 ± 0.18	26.40 ± 0.13	26.46 ± 0.19	26.20 ± 0.13	25.99 ± 0.11	27.47 ± 0.23
213.640	26.87 ± 0.22	26.70 ± 0.16	25.56 ± 0.09	25.69 ± 0.12	25.11 ± 0.08	26.41 ± 0.34
217.940	25.98 ± 0.10	26.86 ± 0.18	25.19 ± 0.07	25.97 ± 0.11	25.57 ± 0.09	25.96 ± 0.09
221.077	26.26 ± 0.12	26.67 ± 0.15	25.33 ± 0.07	26.80 ± 0.18	25.70 ± 0.09	26.04 ± 0.08
225.313	27.07 ± 0.22	25.98 ± 0.10	25.51 ± 0.13	26.66 ± 0.21	25.98 ± 0.12	26.38 ± 0.13
229.922	26.92 ± 0.19	26.51 ± 0.16	25.59 ± 0.14	25.41 ± 0.08	26.04 ± 0.10	26.76 ± 0.15
235.162	26.02 ± 0.12	26.75 ± 0.20	26.11 ± 0.14	25.99 ± 0.14	25.31 ± 0.07	26.92 ± 0.22
241.986	26.49 ± 0.21	26.13 ± 0.11	26.04 ± 0.09	26.41 ± 0.17	25.84 ± 0.10	26.92 ± 0.27
249.763	25.39 ± 0.15	26.78 ± 0.23	25.41 ± 0.07	25.71 ± 0.09	26.18 ± 0.11	26.49 ± 0.17
574.203	26.76 ± 0.14	26.13 ± 0.08	26.31 ± 0.11	26.10 ± 0.10	25.35 ± 0.19	26.11 ± 0.11
2450000+	C25	C26				
189.847	25.37 ± 0.07	25.71 ± 0.10	...	...	...	...
198.024	25.85 ± 0.11	26.45 ± 0.18	...	...	...	...
208.947	25.82 ± 0.10	26.07 ± 0.12	...	...	...	...
211.106	25.22 ± 0.11	26.27 ± 0.12	...	...	...	...
213.640	25.41 ± 0.08	26.56 ± 0.17	...	...	...	...
217.940	25.83 ± 0.11	26.63 ± 0.21	...	...	...	...
221.077	25.86 ± 0.09	26.59 ± 0.26	...	...	...	...
225.313	26.14 ± 0.10	25.88 ± 0.12	...	...	...	...
229.922	26.36 ± 0.16	26.41 ± 0.18	...	...	...	...
235.162	25.42 ± 0.08	26.79 ± 0.22	...	...	...	...
241.986	25.75 ± 0.10	25.84 ± 0.10	...	...	...	...
249.763	26.30 ± 0.11	26.45 ± 0.18	...	...	...	...
574.203	26.16 ± 0.09	26.67 ± 0.17	...	...	...	...

Table 6—Continued

JD	$V \pm \sigma_V$	$V \pm \sigma_V$	$V \pm \sigma_V$	$V \pm \sigma_V$	$V \pm \sigma_V$	$V \pm \sigma_V$

Table 7. ALLFRAME I Photometry for NGC 4548 Cepheids

JD	$I \pm \sigma_V$	$I \pm \sigma_V$	$I \pm \sigma_V$	$I \pm \sigma_V$	$I \pm \sigma_V$	$I \pm \sigma_V$
2450000+	C1	C2	C3	C4	C5	C6
189.943	24.68 ± 0.10	25.39 ± 0.14	25.47 ± 0.13	24.52 ± 0.08	25.26 ± 0.13	25.15 ± 0.16
198.117	25.05 ± 0.10	25.74 ± 0.19	25.08 ± 0.12	24.83 ± 0.08	25.57 ± 0.15	25.87 ± 0.21
209.042	25.21 ± 0.11	25.72 ± 0.20	25.58 ± 0.12	24.68 ± 0.07	25.03 ± 0.11	25.52 ± 0.19
214.067	24.94 ± 0.10	25.63 ± 0.17	25.60 ± 0.14	24.46 ± 0.08	25.12 ± 0.12	25.53 ± 0.16
221.171	24.87 ± 0.10	26.05 ± 0.25	25.47 ± 0.14	24.65 ± 0.08	25.43 ± 0.10	26.24 ± 0.32
230.036	25.21 ± 0.13	25.41 ± 0.10	24.86 ± 0.11	24.90 ± 0.10	25.56 ± 0.13	25.23 ± 0.15
242.079	25.24 ± 0.13	25.91 ± 0.22	25.79 ± 0.21	24.63 ± 0.07	25.34 ± 0.14	25.74 ± 0.43
249.855	24.88 ± 0.17	25.82 ± 0.16	25.00 ± 0.12	24.63 ± 0.08	25.51 ± 0.09	25.31 ± 0.32
2450000+	C7	C8	C9	C10	C11	C12
189.943	25.37 ± 0.27	25.25 ± 0.11	24.48 ± 0.10	25.67 ± 0.30	26.24 ± 0.15	24.76 ± 0.12
198.117	25.81 ± 0.23	25.33 ± 0.13	24.53 ± 0.09	25.41 ± 0.17	25.02 ± 0.11	24.59 ± 0.09
209.042	25.26 ± 0.15	24.93 ± 0.10	24.92 ± 0.11	25.51 ± 0.38	25.86 ± 0.19	24.87 ± 0.08
214.067	25.88 ± 0.26	24.65 ± 0.37	25.20 ± 0.14	24.71 ± 0.25	25.58 ± 0.15	25.05 ± 0.10
221.171	25.69 ± 0.17	24.99 ± 0.10	24.56 ± 0.10	25.62 ± 0.14	25.15 ± 0.11	24.41 ± 0.08
230.016	25.71 ± 0.18	25.14 ± 0.10	24.61 ± 0.08	25.33 ± 0.11	25.39 ± 0.12	24.56 ± 0.10
242.079	25.25 ± 0.13	25.01 ± 0.10	24.78 ± 0.09	26.17 ± 0.30	25.11 ± 0.12	25.08 ± 0.11
249.885	25.87 ± 0.19	25.17 ± 0.11	25.25 ± 0.10	25.20 ± 0.10	25.39 ± 0.14	24.35 ± 0.08
2450000+	C13	C14	C15	C16	C17	C18
189.943	25.82 ± 0.21	24.85 ± 0.10	25.22 ± 0.11	25.35 ± 0.12	25.63 ± 0.16	24.92 ± 0.14
198.117	25.10 ± 0.14	24.87 ± 0.09	25.78 ± 0.23	25.35 ± 0.15	25.58 ± 0.15	25.24 ± 0.17
209.042	25.39 ± 0.15	24.42 ± 0.08	25.34 ± 0.17	25.14 ± 0.12	26.48 ± 0.37	25.48 ± 0.19
214.067	25.61 ± 0.17	24.66 ± 0.13	25.80 ± 0.24	25.27 ± 0.12	25.37 ± 0.11	25.35 ± 0.34
221.171	25.36 ± 0.17	24.91 ± 0.10	26.02 ± 0.17	25.09 ± 0.11	25.95 ± 0.26	24.73 ± 0.10
230.016	25.80 ± 0.26	24.73 ± 0.08	25.42 ± 0.15	25.40 ± 0.15	25.57 ± 0.14	25.02 ± 0.14
242.079	25.35 ± 0.13	24.61 ± 0.08	25.23 ± 0.11	25.23 ± 0.12	25.38 ± 0.26	25.59 ± 0.13
249.885	26.00 ± 0.23	24.92 ± 0.15	25.72 ± 0.16	25.30 ± 0.12	25.26 ± 0.12	25.33 ± 0.15
2450000+	C19	C20	C21	C22	C23	C24
189.943	25.73 ± 0.17	25.18 ± 0.10	24.58 ± 0.09	25.71 ± 0.16	25.27 ± 0.12	25.18 ± 0.14
198.117	25.80 ± 0.19	25.56 ± 0.16	24.88 ± 0.12	25.01 ± 0.10	24.86 ± 0.09	24.15 ± 0.13
209.042	25.72 ± 0.18	25.20 ± 0.16	25.45 ± 0.17	25.56 ± 0.14	24.93 ± 0.10	25.06 ± 0.12
214.067	25.86 ± 0.36	25.76 ± 0.17	24.70 ± 0.08	25.28 ± 0.15	24.78 ± 0.10	24.69 ± 0.11
221.171	25.36 ± 0.12	26.17 ± 0.27	24.56 ± 0.10	25.27 ± 0.15	25.08 ± 0.12	25.00 ± 0.13
230.016	25.89 ± 0.21	25.76 ± 0.18	24.86 ± 0.09	25.07 ± 0.12	25.19 ± 0.15	25.38 ± 0.20
242.079	25.87 ± 0.22	25.06 ± 0.13	25.51 ± 0.13	25.51 ± 0.14	25.08 ± 0.14	24.83 ± 0.12

Table 7—Continued

JD	$I \pm \sigma_V$	$I \pm \sigma_V$	$I \pm \sigma_V$	$I \pm \sigma_V$	$I \pm \sigma_V$	$I \pm \sigma_V$
249.885	25.03 ± 0.09	25.76 ± 0.16	24.37 ± 0.08	25.13 ± 0.13	25.21 ± 0.12	25.04 ± 0.13
2450000+	C25	C26				
189.943	24.69 ± 0.08	25.22 ± 0.13	...	...	...	...
198.117	25.07 ± 0.10	25.77 ± 0.23	...	...	...	...
209.042	24.79 ± 0.09	25.17 ± 0.14	...	...	...	...
214.067	24.89 ± 0.09	25.46 ± 0.19	...	...	...	...
221.171	24.93 ± 0.09	25.32 ± 0.18	...	...	...	...
230.016	25.40 ± 0.14	25.49 ± 0.16	...	...	...	...
242.079	24.77 ± 0.07	25.09 ± 0.16	...	...	...	...
249.885	25.18 ± 0.11	25.51 ± 0.14	...	...	...	...

Table 8. Positions and Mean Magnitudes for Other Variable Stars

Star	Chip	x	y	R.A.(2000) h m s	Dec.(2000) ° ′ ″	$< V >$	$< I >$	Notes
V01	3	720.46	531.16	12 35 23.64	14 29 02.16	26.22	25.63	Prob. Ceph. P=$16^d.2$
V02	3	711.12	565.65	12 35 23.65	14 29 05.69	25.90	25.97	Blue
V03	2	211.93	540.57	12 35 25.73	14 28 02.91	25.61	24.84	Poss. Ceph. P=$26^d.0$
V04	2	138.04	429.69	12 35 26.37	14 28 12.48	25.63	24.63	No good period
V05	3	211.13	340.17	12 35 27.32	14 28 54.43	25.96	24.98	Prob. Ceph. P=$24^d.8$
V06	1	265.56	369.23	12 35 29.82	14 28 17.78	25.18	25.33	Blue
V07	1	266.04	635.60	12 35 30.00	14 28 05.98	24.44	23.30	Small variation
V08	4	417.91	438.86	12 35 31.04	14 29 13.97	22.13	21.80	Blue supergiant vbl?
V09	4	113.37	486.37	12 35 31.78	14 28 45.34	25.32	24.94	Poss. Ceph. P=$24^d.1$

Table 9. Periods/Mean Magnitudes for Cepheid Variables

Star	P (days)	logP	$< V >_i^{ALL}$	$< V >_{ph}^{ALL}$	$< I >_i^{ALL}$	$< I >_{ph}^{ALL}$	$< V >_{ph}^{DoP}$	$< I >_{ph}^{DoP}$
C01	33.2	1.521	26.18	26.20	24.99	25.00	26.03	24.83
C02	18.4	1.265	26.46	26.53	25.68	25.72	26.31	25.47
C03	24.8	1.394	26.08	26.07	25.32	25.28	25.98	25.07
C04	29.5	1.469	25.47	25.53	24.65	24.68	25.50	24.63
C05	24.2	1.384	26.30	26.37	25.33	25.33	26.28	25.13
C06	19.1	1.281	26.56	26.58	25.53	25.64	26.45	25.42
C07	17.1	1.233	26.39	26.37	25.57	25.59	26.19	25.32
C08	31.0	1.491	26.23	26.19	25.04	25.02	26.13	25.03
C09	38.2	1.582	25.97	25.98	24.76	24.72	25.88	24.56
C10	18.8	1.274	25.96	26.07	25.38	25.42	25.96	25.23
C11	23.7	1.375	26.31	26.36	25.40	25.41	26.21	25.15
C12	29.4	1.468	25.68	25.78	24.68	24.70	25.68	25.07
C13	18.0	1.255	26.77	26.68	25.52	25.43	26.70	...
C14	31.0	1.491	25.56	25.54	24.73	24.71	25.55	24.55
C15	17.5	1.243	26.13	26.25	25.53	25.60	26.31	25.34
C16	29.2	1.465	26.04	26.07	25.26	25.26	26.07	25.33
C17	17.5	1.243	26.64	26.64	25.60	25.70	26.64	25.64
C18	35.0	1.544	26.50	26.55	25.17	25.16	26.58	25.26
C19	16.5	1.217	26.44	26.37	25.61	25.52	26.67	25.61
C20	17.5	1.242	26.39	26.48	25.50	25.57	26.54	25.68
C21	28.2	1.450	25.74	25.76	24.80	24.87	25.80	24.74
C22	16.9	1.228	26.07	26.10	25.29	25.29	26.14	25.04
C23	21.2	1.326	25.69	25.72	25.04	25.02	25.71	24.86
C24	20.2	1.305	25.88	25.86	25.00	24.92	25.91	24.84
C25	23.3	1.367	25.72	25.78	24.94	24.95	25.79	24.89
C26	17.0	1.230	26.28	26.29	25.36	25.35	26.27	25.30

Table 10. Error Budget

	Source of Uncertainty	Error	Comment
(a)	F555W calibration	± 0.04	
(b)	F814W calibration	± 0.08	
(c)	V photometry zero	± 0.03	
(d)	I photometry zero	± 0.04	
(A)	**cumulative error V**	**± 0.05**	(errors uncorrelated)
(B)	**cumulative error I**	**± 0.09**	
(e)	PL fit (V)	± 0.07	
(f)	PL fit (I)	± 0.05	
(C)	**True Modulus**	**± 0.23**	due to A,B,e,f (errors correlated)
(g)	LMC Modulus	± 0.10	(systematic)
(h)	V PL zero point	± 0.05	
(i)	I PL zero point	± 0.05	
(D)	**Systematic Uncertainty**	**± 0.12**	g,h,i
(E)	**Total Uncertainty**	**± 0.26**	C,D

Table 11. Cepheid Distances to Galaxies in Virgo

Galaxy	RSA Type	Δ(°)	d (Mpc)	Reference
NGC 4321	Sc(s)I	3.6	16.1 ± 1.3	Ferrarese*et al.* (1996)
NGC 4496A	SBcIII-IV	8.7	16.1 ± 1.1	Saha *et al.* (1996b)
NGC 4535	SBc(s)I.3	4.6	16.3 ± 1.3	Macri *et al.* (1998)
NGC 4536	Sc(s)I.3	10.5	16.6 ± 1.2	Saha *et al.* (1996a)
NGC 4548	SBb(rs)I-II	2.2	16.1 ± 2.0	This paper
NGC 4571	Sc(s)II-III	2.2	14.9 ± 1.2	Pierce *et al.* (1994)
NGC 4639	SBb(r)II	3.1	{25.5 ± 2.6	Saha *et al.* (1997)
			{23.6 ± 1.5	Gibson *et al.* (1998)

REFERENCES

Aaronson, M. & Mould, J. 1986, ApJ, 303, 1

Binggeli, B., Tammann, G.A. & Sandage, A. 1987, AJ94, 251

Böhm-Vitense, E. 1988, ApJ, 324, L27

Böhringer, H., Neumann, D.M., Schindler, S. & Huchra, J.P. 1997, ApJ 485, 439

Cardelli, J.A., Clayton, G.C.,& Mathis, J.S. 1989, ApJ, 345, 245

de Vaucouleurs, G. & de Vaucouleurs, A. 1973, A&A, 28, 109

de Vaucouleurs, G. *et al.* 1975, Reference Catalogue of Bright Galaxies (Springer-Verlag, New York)

Feast, M.W. & Catchpole, R.M. 1997, MNRAS, 286, L1

Ferrarese, L. *et al.* 1996, ApJ, 464, 568

Ferrarese, L. *et al.* 1998, ApJ, (in press)

Freedman, W.L. 1988, ApJ, 326, 691

Freedman, W.L., & Madore, B.F. 1990, ApJ, 365, 186

Freedman, W.L. *et al.* 1990, ApJ, 355, L35

Freedman, W.L. *et al.* 1994, ApJ, 427, 628

Gibson, B.K. *et al.* 1998 (in preparation)

Graham, J.A. *et al.* 1997, ApJ, 477, 535

Harris, W. 1990, PASP, 102, 966

Hill, R.J. *et al.* 1998, ApJ, 496, 648

Ho, L.C., Filippenko, A.V. & Sargent, W.L.W. 1995, ApJS, 98, 477

Holtzman, J.A. *et al.* 1995a, PASP, 107, 156

Holtzman, J.A. *et al.* 1995b, PASP, 107, 1065

Huchra, J.P. 1985, in The Virgo cluster, eds Richter & Bingelli (ESO, Garching), p 181

Jacoby, G.H., Ciardullo, R. & Ford, H.C. 1990, ApJ, 356, 332

Kennicutt, R.C., Freedman, W.L., & Mould, J.R. 1995, AJ, 110, 1476

Lafler, J., & Kinman, T.D. 1965, ApJS, 11, 216

Macri, L. *et al.* 1998 (in preparation)

Madore, B.F. 1985, in Cepheids: Theory and Observation (IAU Colloquium 82), ed. Madore (Cambridge University Press), p 166

Madore, B.F., & Freedman, W.L. 1991, PASP, 103, 933

Madore, B.F., & Freedman, W.L. 1998, ApJ, 492, 110

Mallas, J.H., & Kreimer, E. in The Messier Album (Sky Publishing Corporation, Cambridge), p 168

McGonegal, R. *et al.* 1985, ApJ, 257, L33

Mould, J. *et al.* 1995, ApJ, 449, 413

Nemec, J.M., & Lutz, T.E. 1993, in New Perspectives on Stellar Pulsation and Pulsating Variable Stars (IAU Colloquium 139) eds Nemec and Matthews (Cambridge University Press) p 31

Pierce, M.J. *et al.* 1994, Nature, 371, 385

Pierce, M.J. & Tully, R.B. 1988, ApJ, 330, 579

Rubin, V.C., Waterman, A.H. & Kenney, J.P.D. 1999, AJ, (submitted)

Saha, A., & Hoessel, J.G. 1990a, ApJ, 330, 579

Saha, A., & Hoessel, J.G. 1990b, AJ, 99, 97

Saha, A. *et al.* 1994, ApJ, 425, 14

Saha, A. *et al.* 1996a, ApJ, 466, 55

Saha, A. *et al.* 1996b, ApJS, 107,693

Saha, A. *et al.* 1997, ApJ, 486, 1

Sandage, A., & Bedke, J. 1994, in The Carnegie Atlas of Galaxies (Carnegie Institution of Washington, Washington DC)

Sandage, A., & Tammann, G. 1981, in A Revised Shapley-Ames Catalogue of Bright Galaxies (Carnegie Institution of Washington, Washington DC)

Schechter, P.L., Mateo, M., & Saha, A. 1993, PASP, 105, 1342

Stellingwerf, R.F. 1978, ApJ, 224, 953

Stetson, P.B. 1990, PASP, 102, 932

Stetson, P.B. 1994, PASP, 106, 250

Stetson, P.B. 1996, PASP, 108, 851

Wayman, P.A., Stift, M.J., & Butler, C.J. 1984, A& AS, 56, 169

Welch, D.L. & Stetson, P.B. 1993, AJ, 105, 1813

Whitmore, B. and Heyer, I. 1997, Instrument Science Report WFPC2 97-08 (STScI, Baltimore)

van den Bergh, S. 1976, ApJ, 206, 883

This manuscript was prepared with the AAS LaTeX macros v4.0.

Fig. 1.— An R image of NGC 4548 with the Hubble Space Telescope field marked. It is adapted from a CCD image taken with the 1.2 m telescope of the F.L. Whipple Observatory on Mount Hopkins, Arizona. The long side of the L-shaped HST footprint is 150″. The PC chip (chip 1) covers the smallest field of the 4 chips. Moving anti-clockwise, the other 3 WF2 fields correspond to chips 2,3 and 4.

Fig. 2.— Sampling variance of light curves from data taken using the exposure sequence given in Table 1. The variance plotted is a measure of the amount by which the observed phase sampling deviates from that of uniform phase sampling. The variance is normalized such the zero variance corresponds to the case where the light curve is unformly sampled. The 1997 revisit observation is not included in this calculation.

Fig. 3.— ALLFRAME − DoPHOT magnitude differences plotted against ALLFRAME magnitude for both bright reference stars and Cepheid variables in each of the 4 chips. Open triangles correspond to chip 1, filled triangles to chip 2, open circles to chip 3 and filled circles to chip 4.

Fig. 4.— Deep HST F555W images of NGC 4548 obtained by combining with median filtering all F555W epochs. The 26 Cepheids and the additional 9 variables are identified on each of the chips. The vignetted edges of each field are shown masked.

Fig. 5.— Finding charts for the Cepheids listed in Table 5 Each finding chart covers a 5″× 5″region and has the same orientation as the corresponding chips in Figure 4. The contrast and intensity have been adjusted differently for each finding chart, therefore the relative brightness of the Cepheids cannot be inferred from them.

Fig. 6.— Finding charts for the additional variable stars listed in Table 8. Each finding chart covers a 5″× 5″region and has the same orientation as the corresponding chips in Figure 4.

Fig. 7.— ALLFRAME V magnitude light curves for each Cepheid variable. The adopted period is shown along with a characteristic uncertainty range as reported by ALLFRAME for a typical point.

Fig. 8.— An I, $V-I$ color magnitude diagram constructed using the mean photometric magnitudes of all stars measured in ALLFRAME. Cepheid are shown as filled circles and populate the instability strip.

Fig. 9.— The V PL relation for the sample of Cepheids. The solid line represents the best unweighted fit using phase weighted mean magnitudes and corresponds to a modulus of 31.31±0.07 mag. The dashed lines drawn at ±0.54 mag reflect the finite width of the Cepheid instability strip.

Fig. 10.— The I PL relation for the sample of Cepheids. The solid line represents the best unweighted fit using phase weighted mean magnitudes and corresponds to a modulus of 31.20±0.05 mag. The dashed lines drawn at ±0.36 mag reflect the finite width of the Cepheid instability strip.

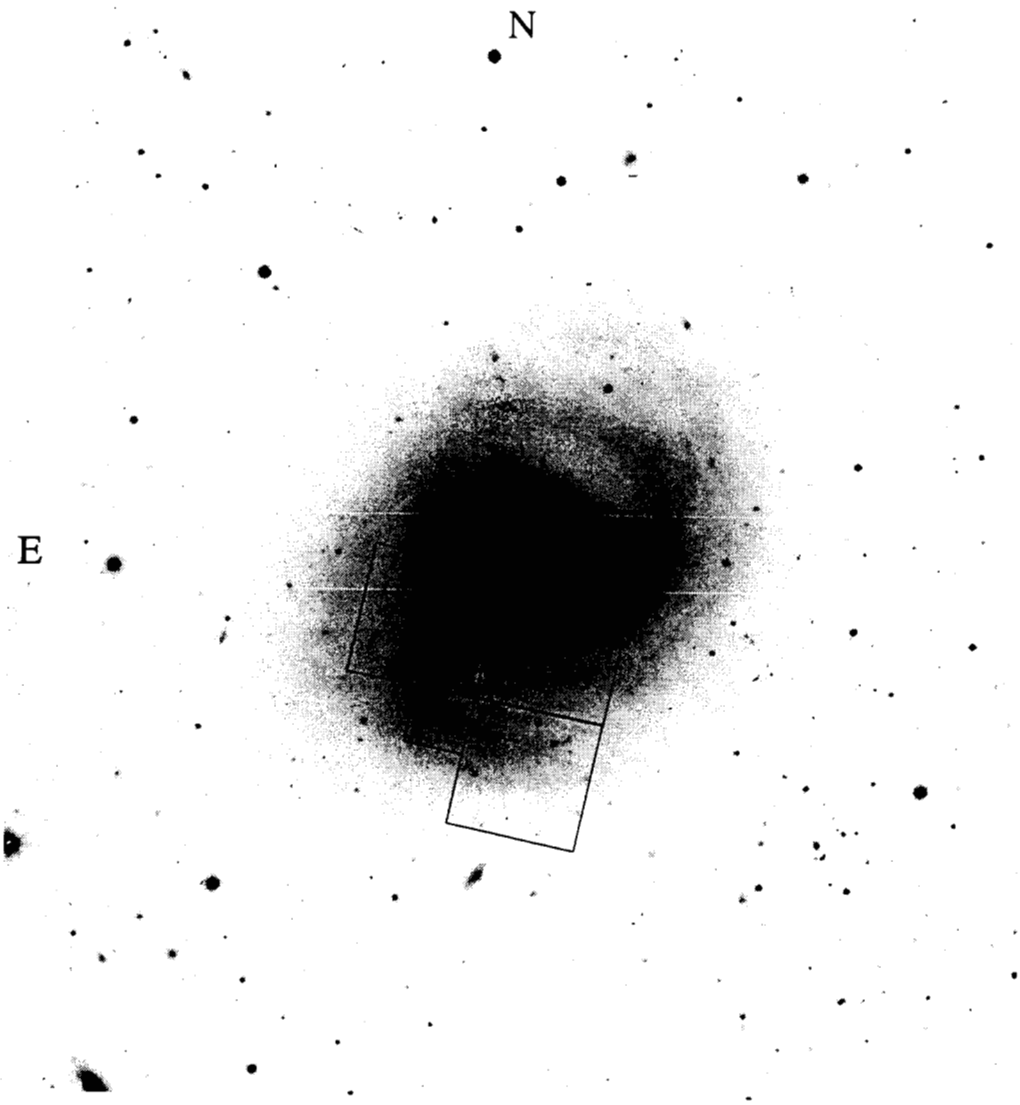

Figure 1

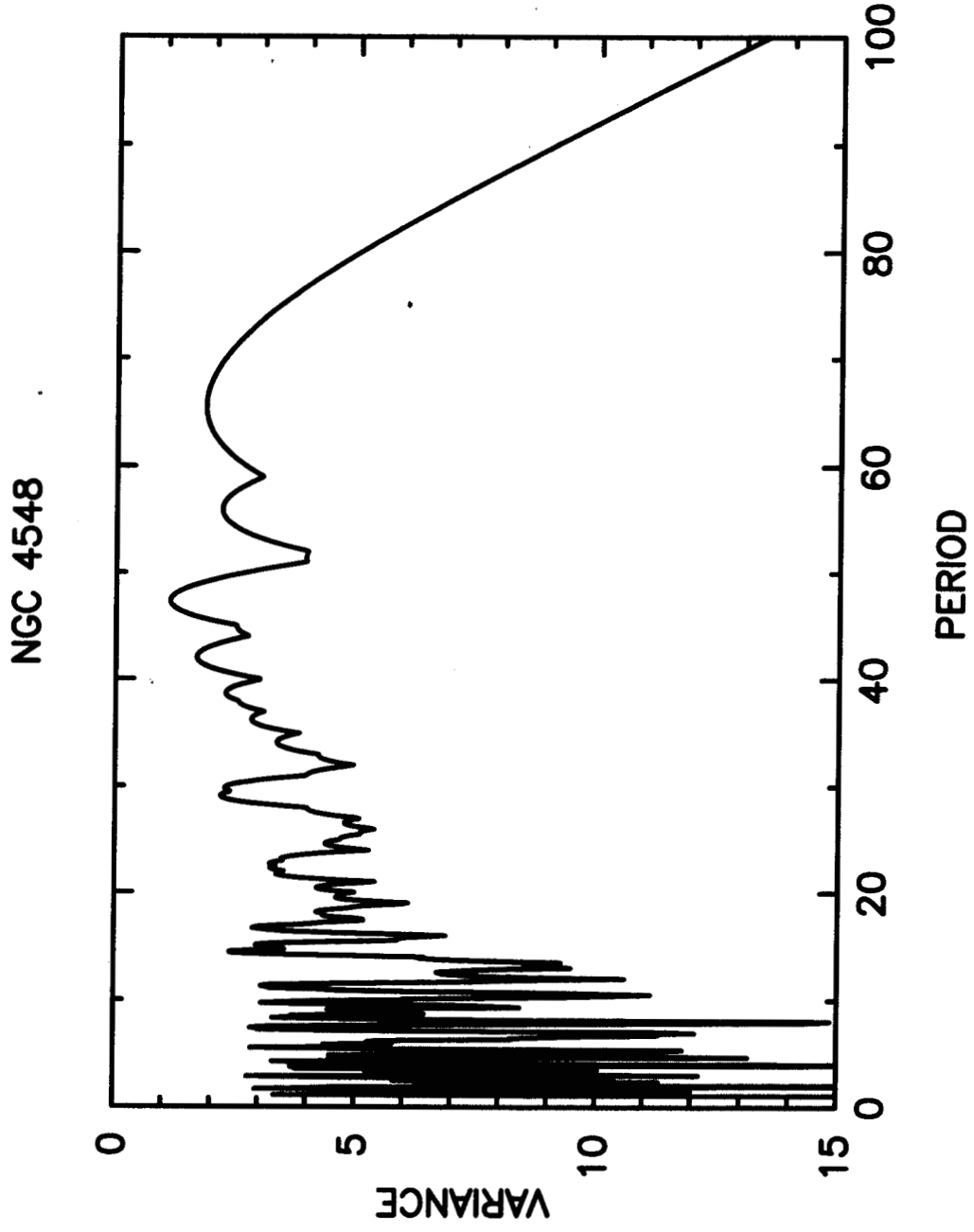

Figure 2

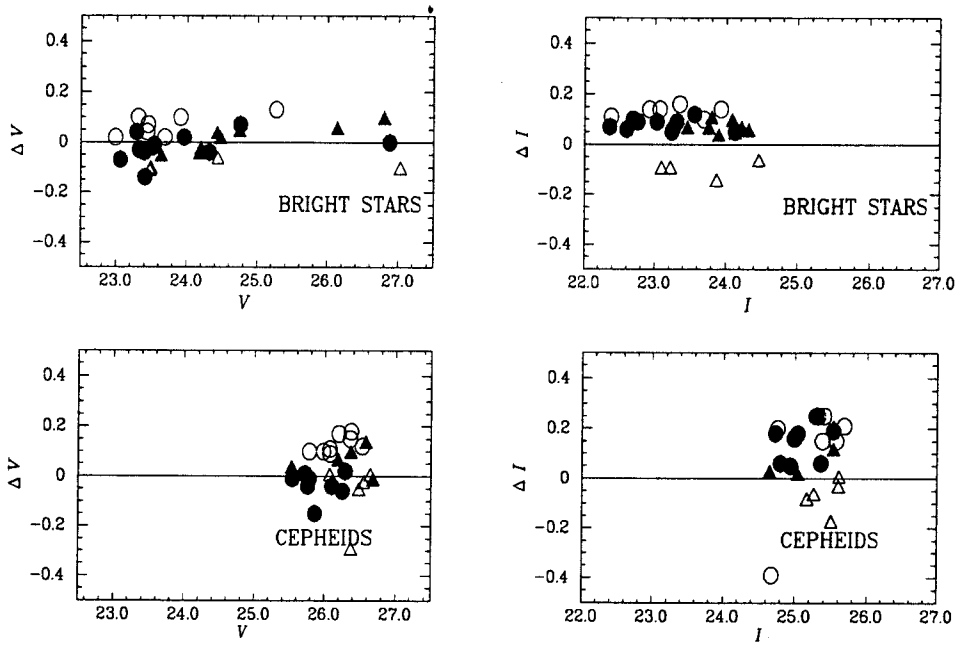

Figure 3

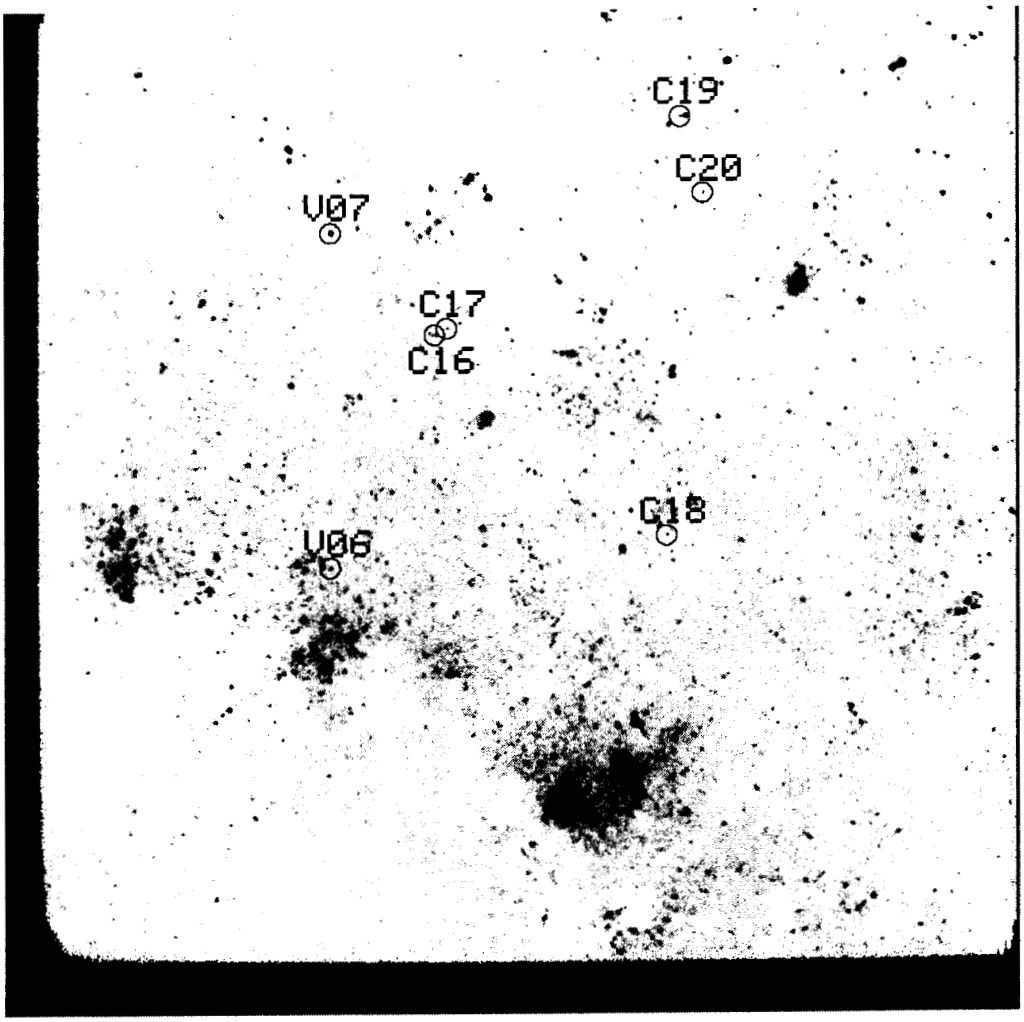

Figure 4a

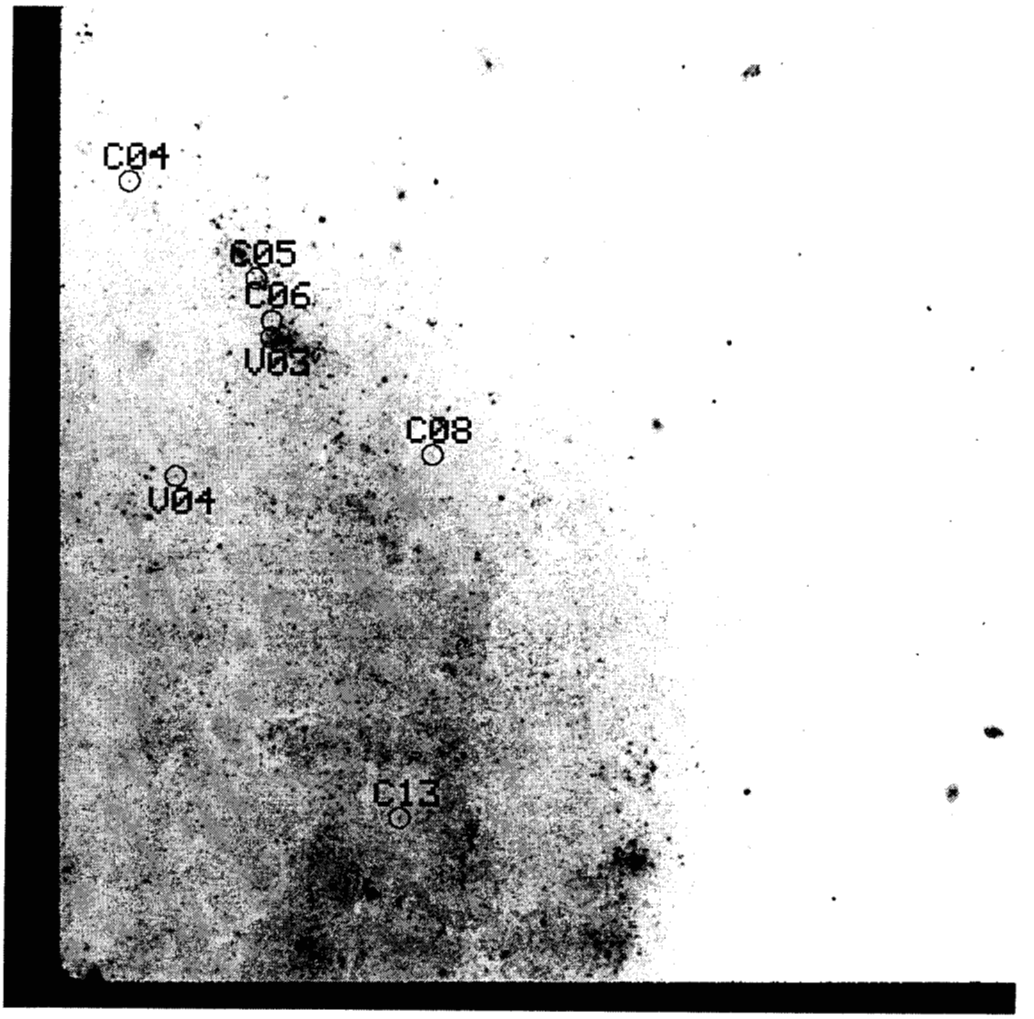

Figure 4b

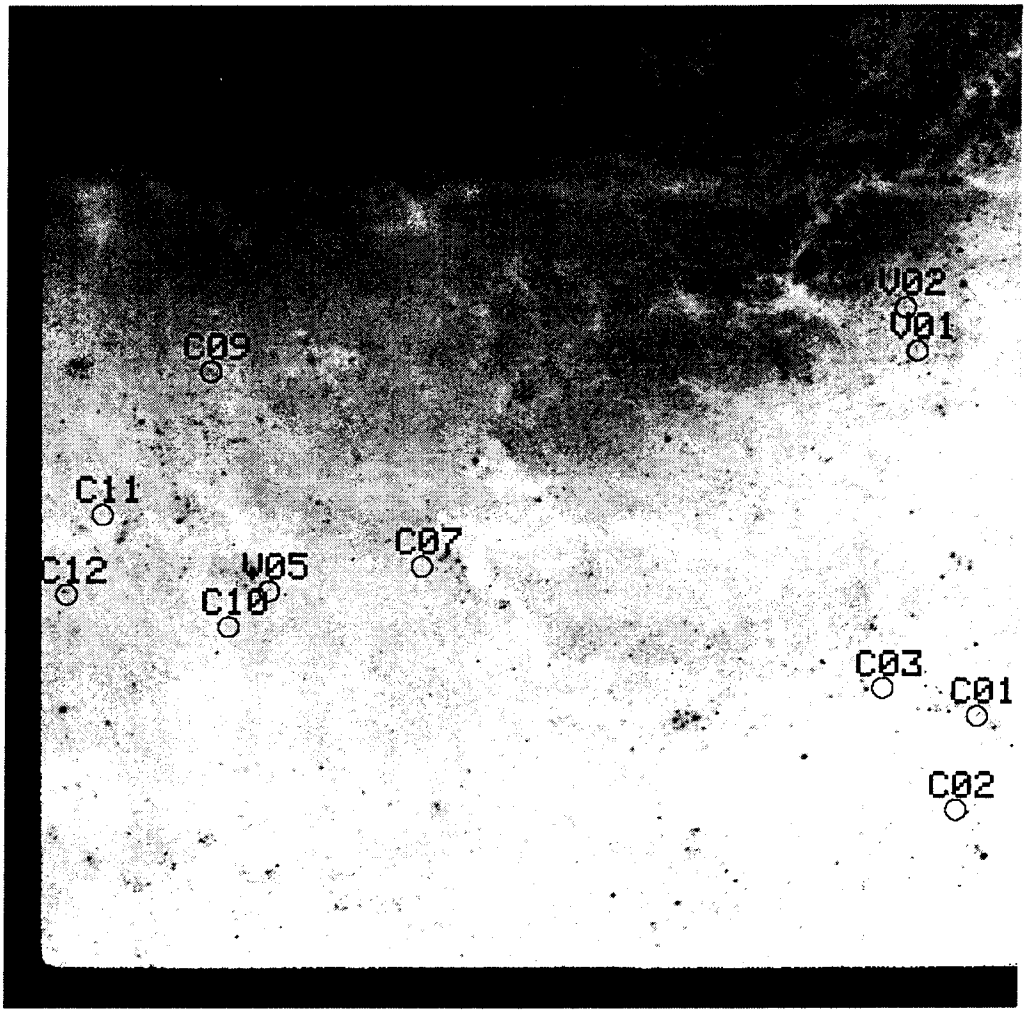

Figure 4c

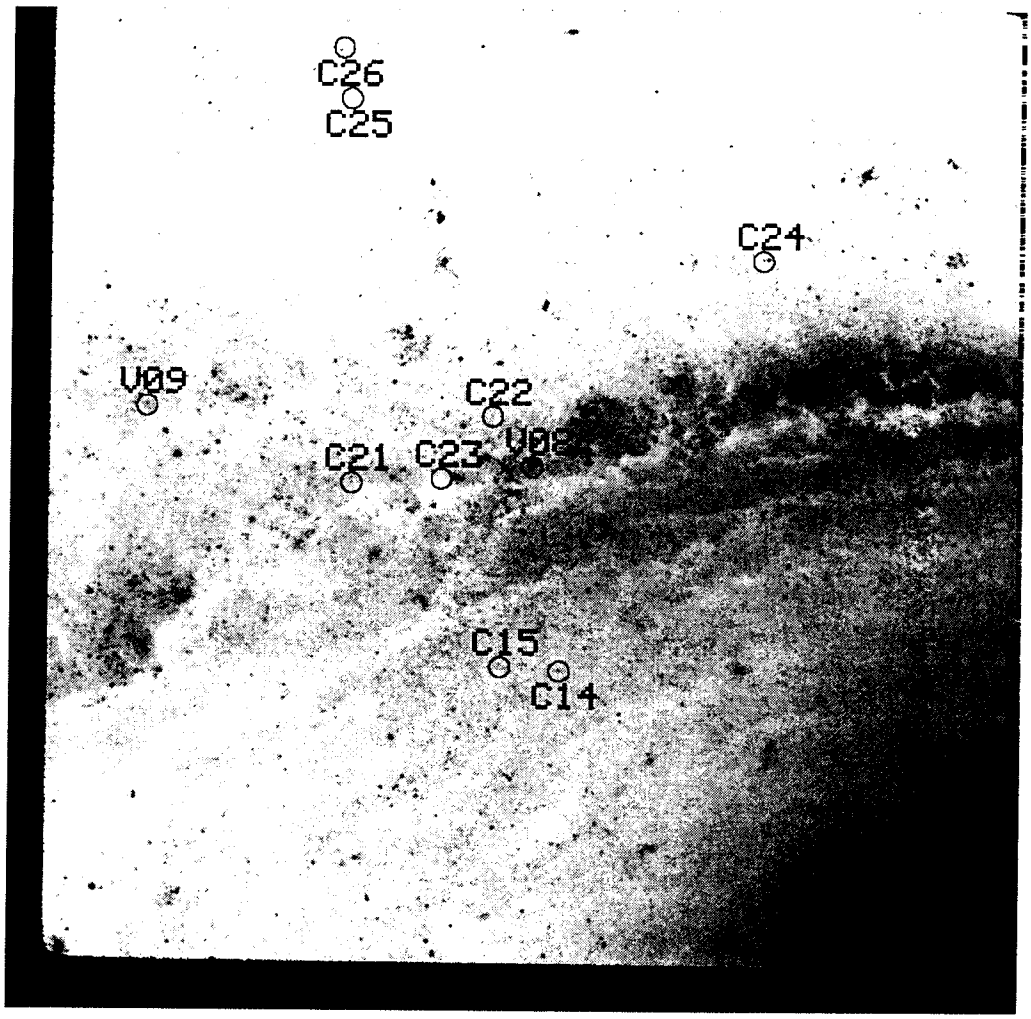

Figure 4d

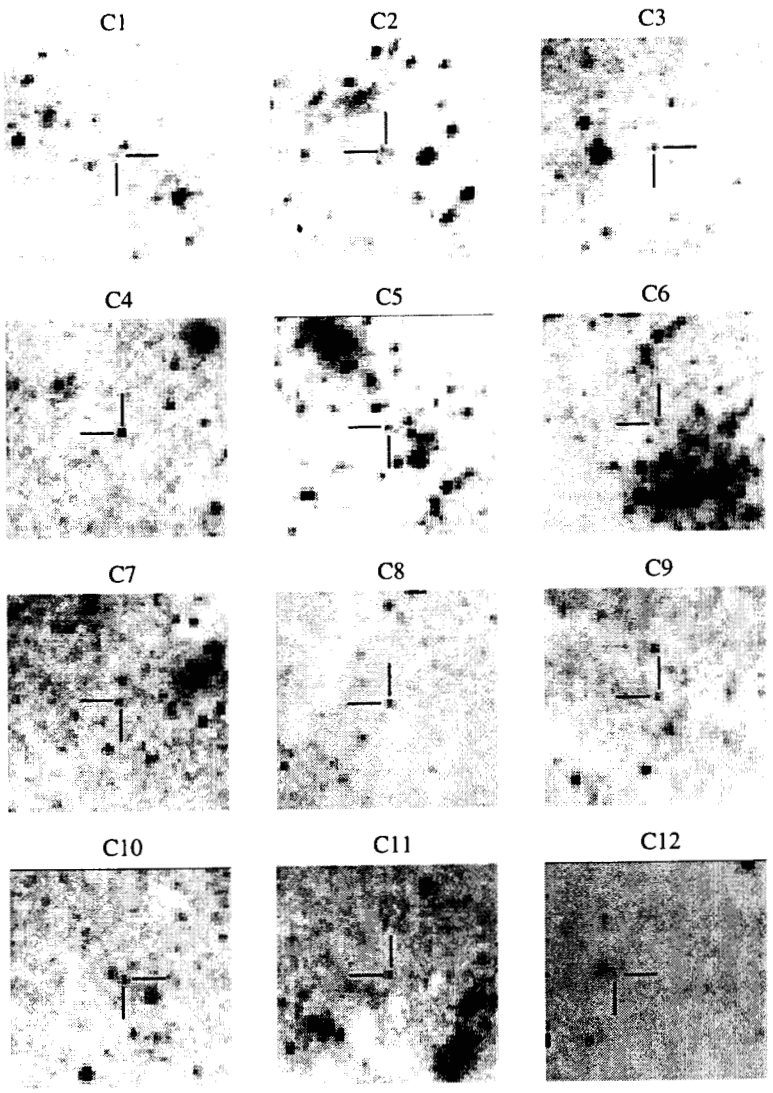

Figure 5a

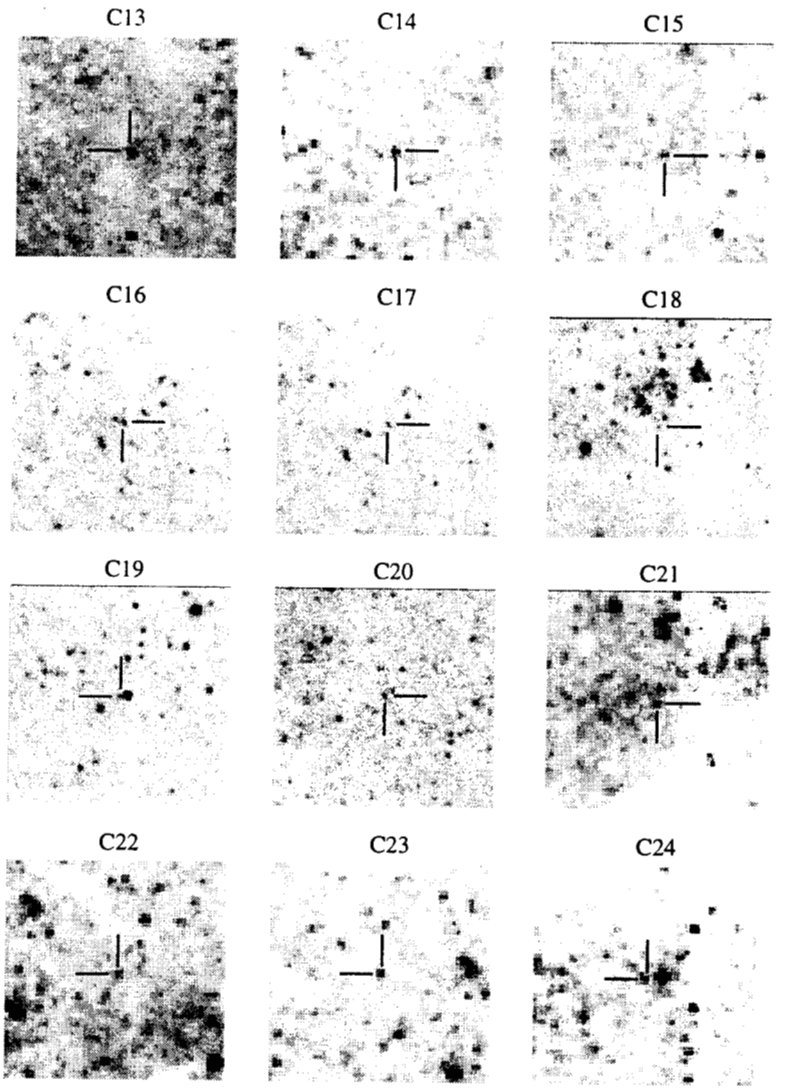

Figure 5b

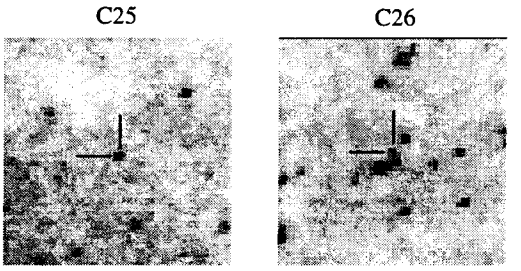

Figure 5c

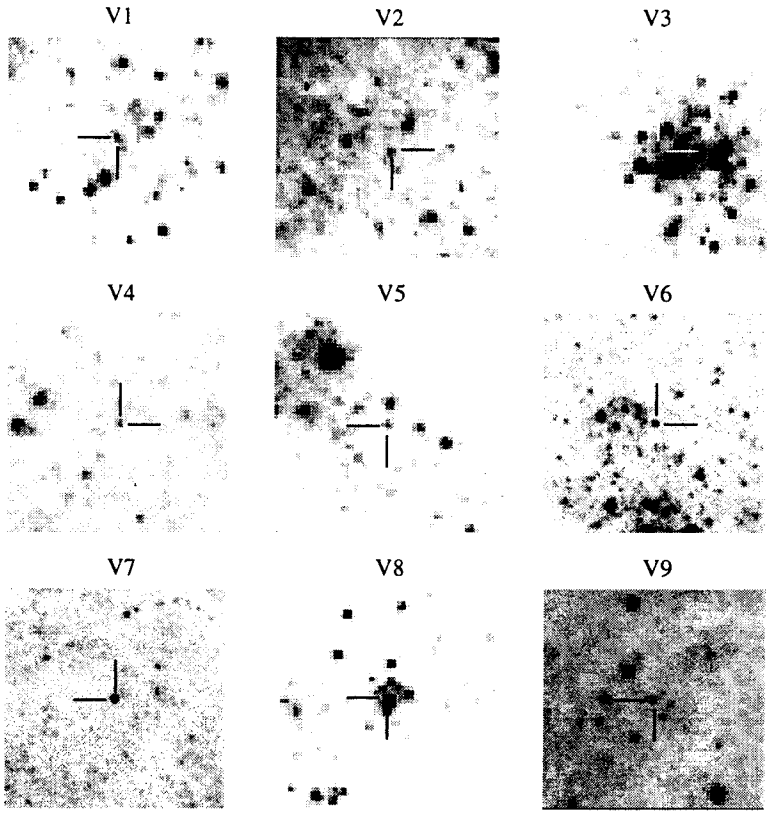

Figure 6

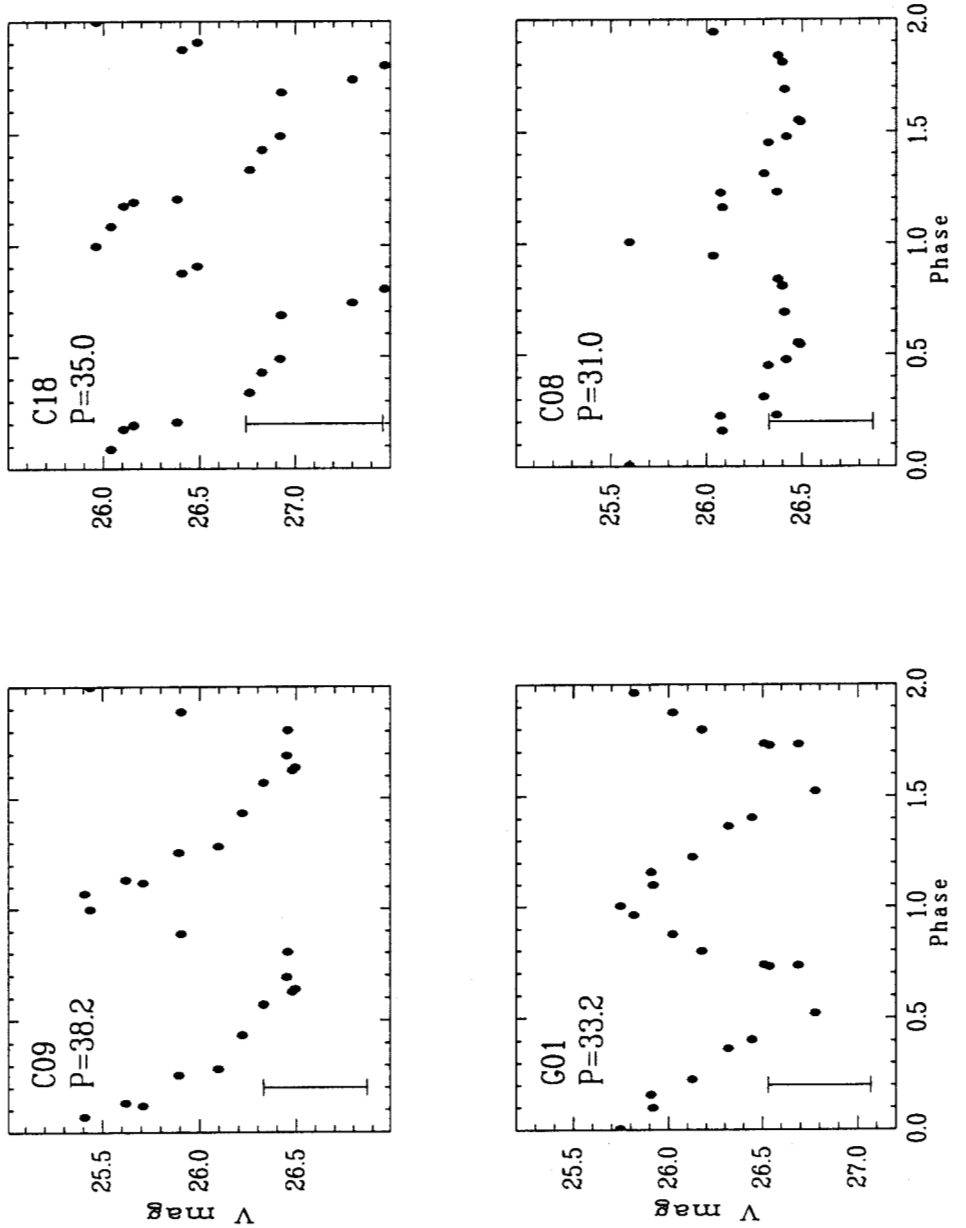
C18
P=35.0
C08
P=31.0
C09
P=38.2
G01
P=33.2
V mag
Phase
25.5
26.0
26.5
27.0
0.0
0.5
1.0
1.5
2.0

Figure 7a

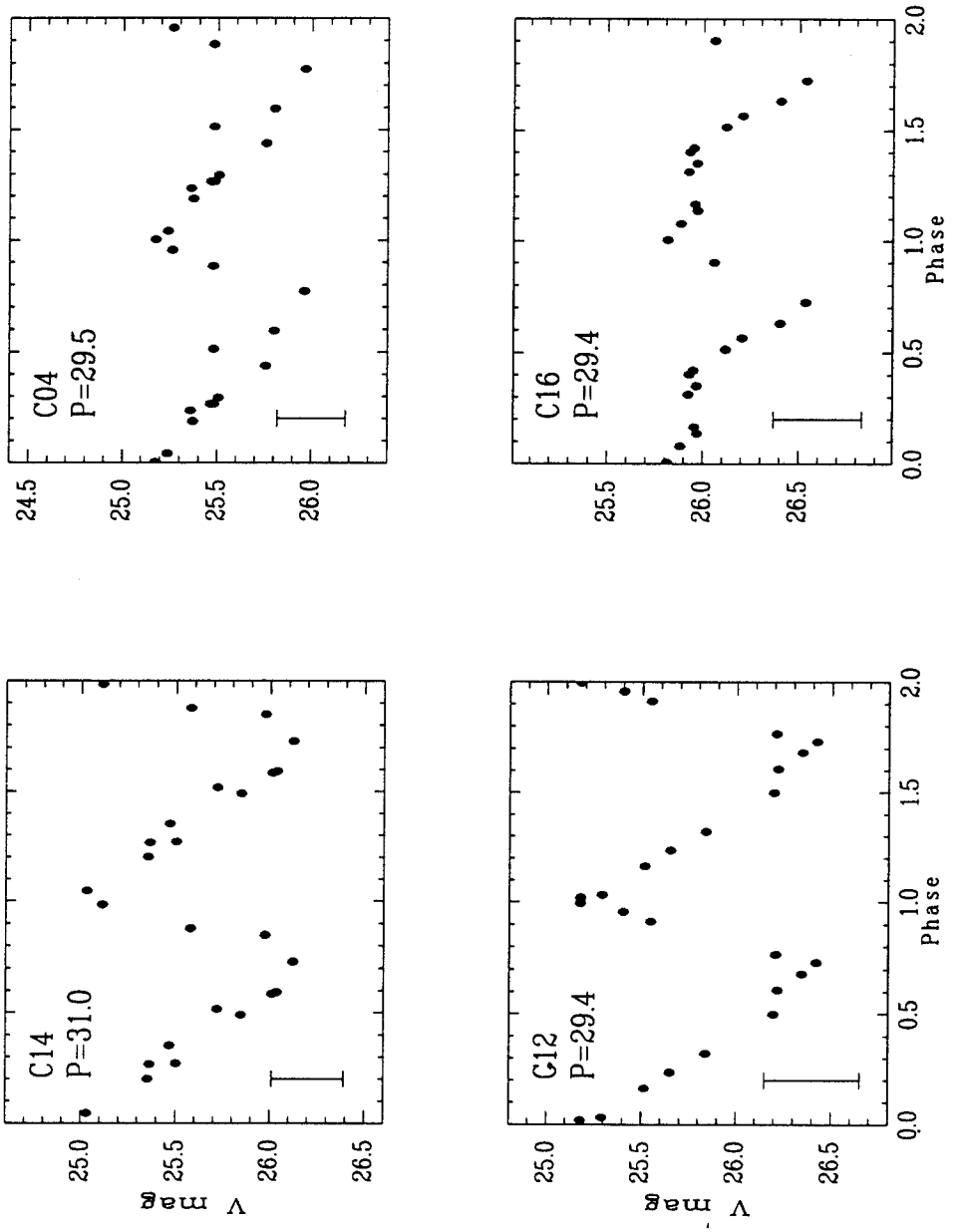

Figure 7b

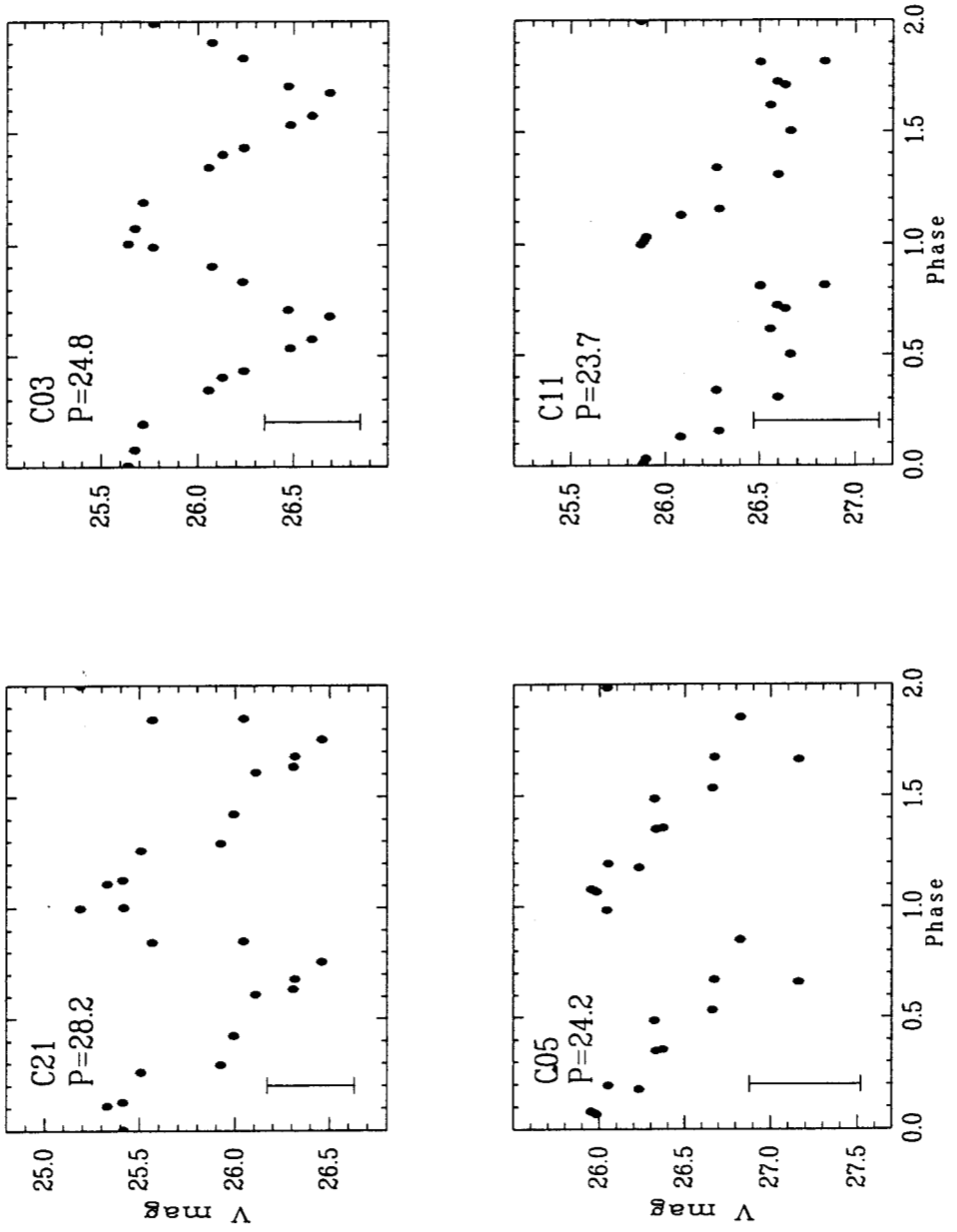

Figure 7c

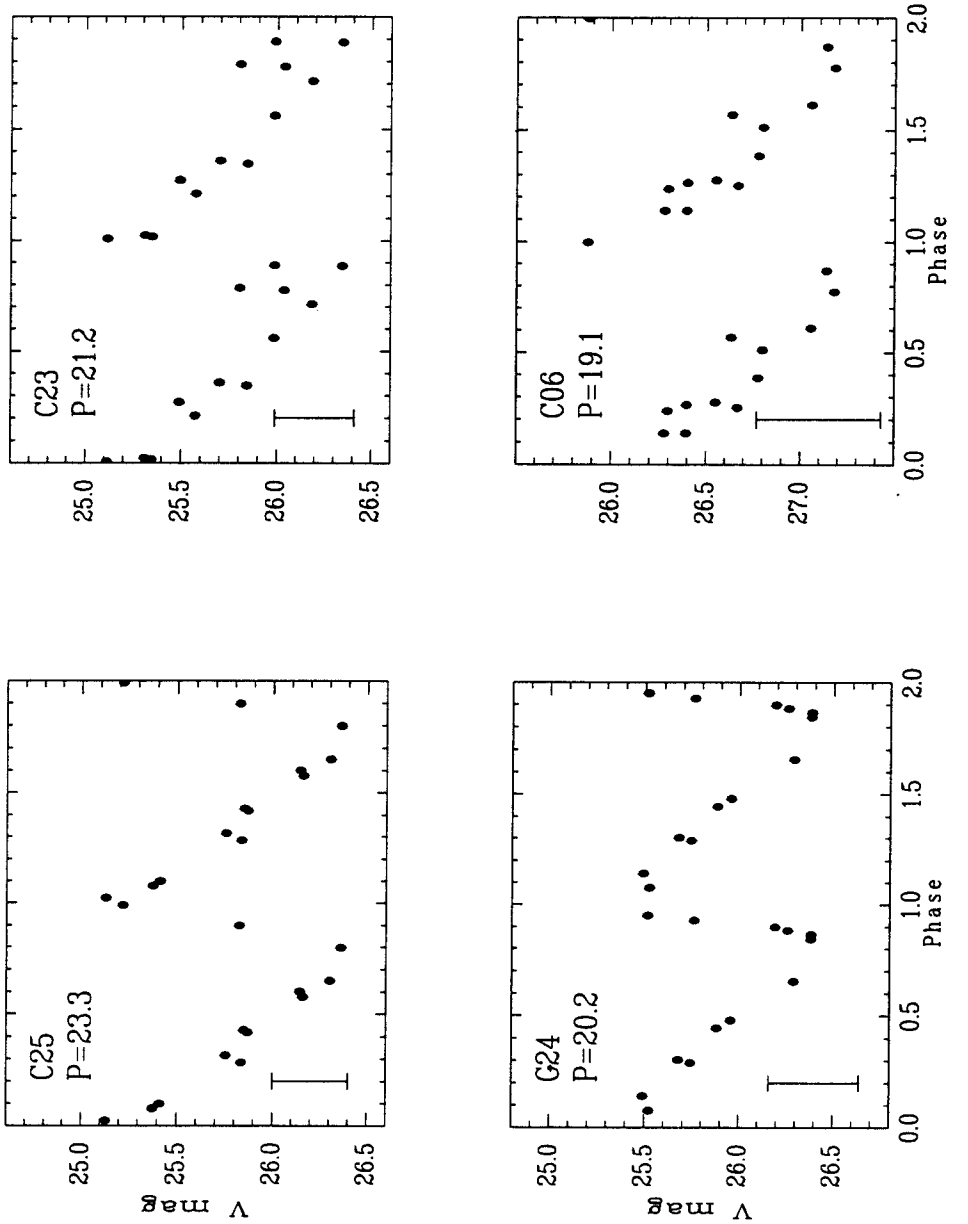

Figure 7d

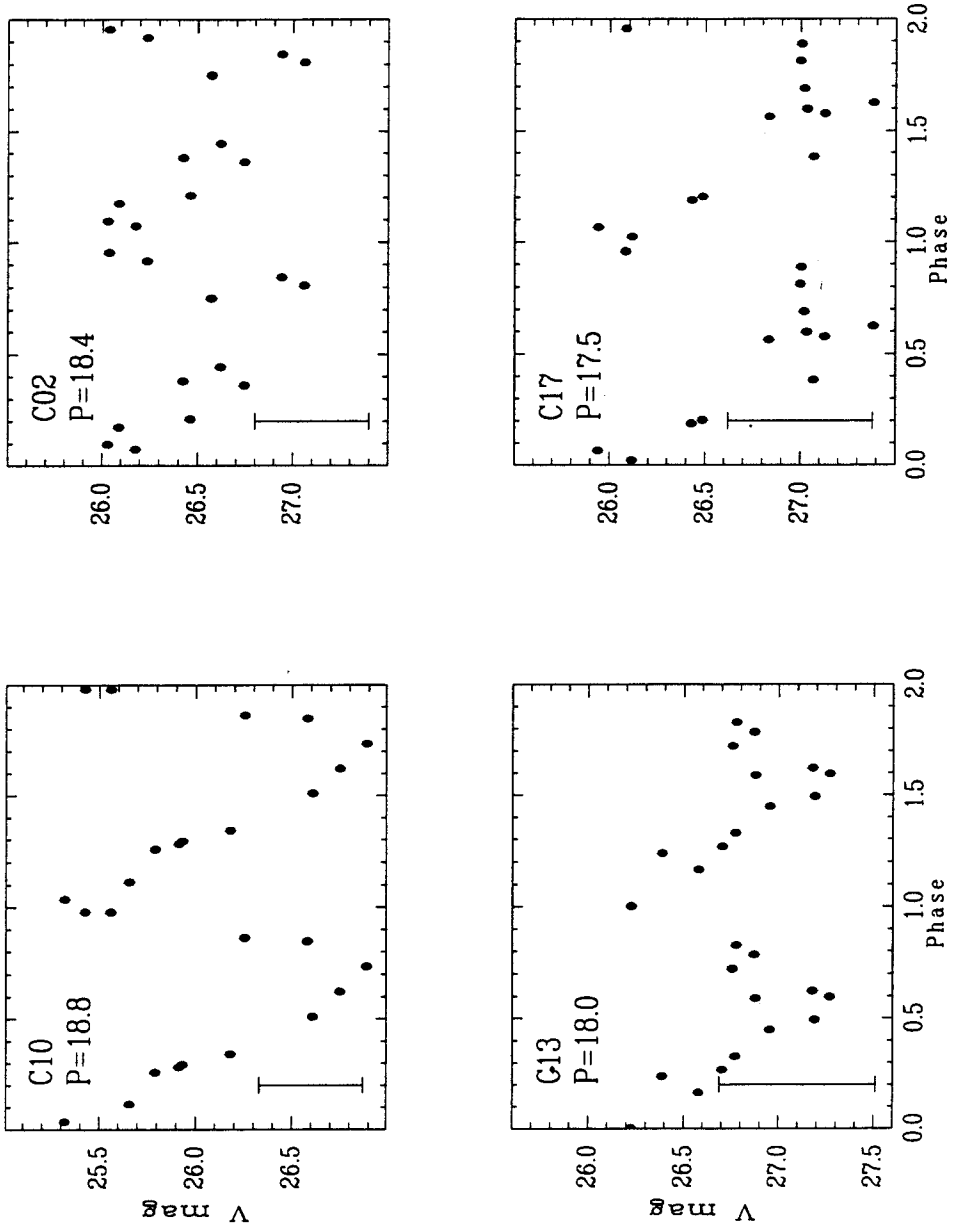

Figure 7e

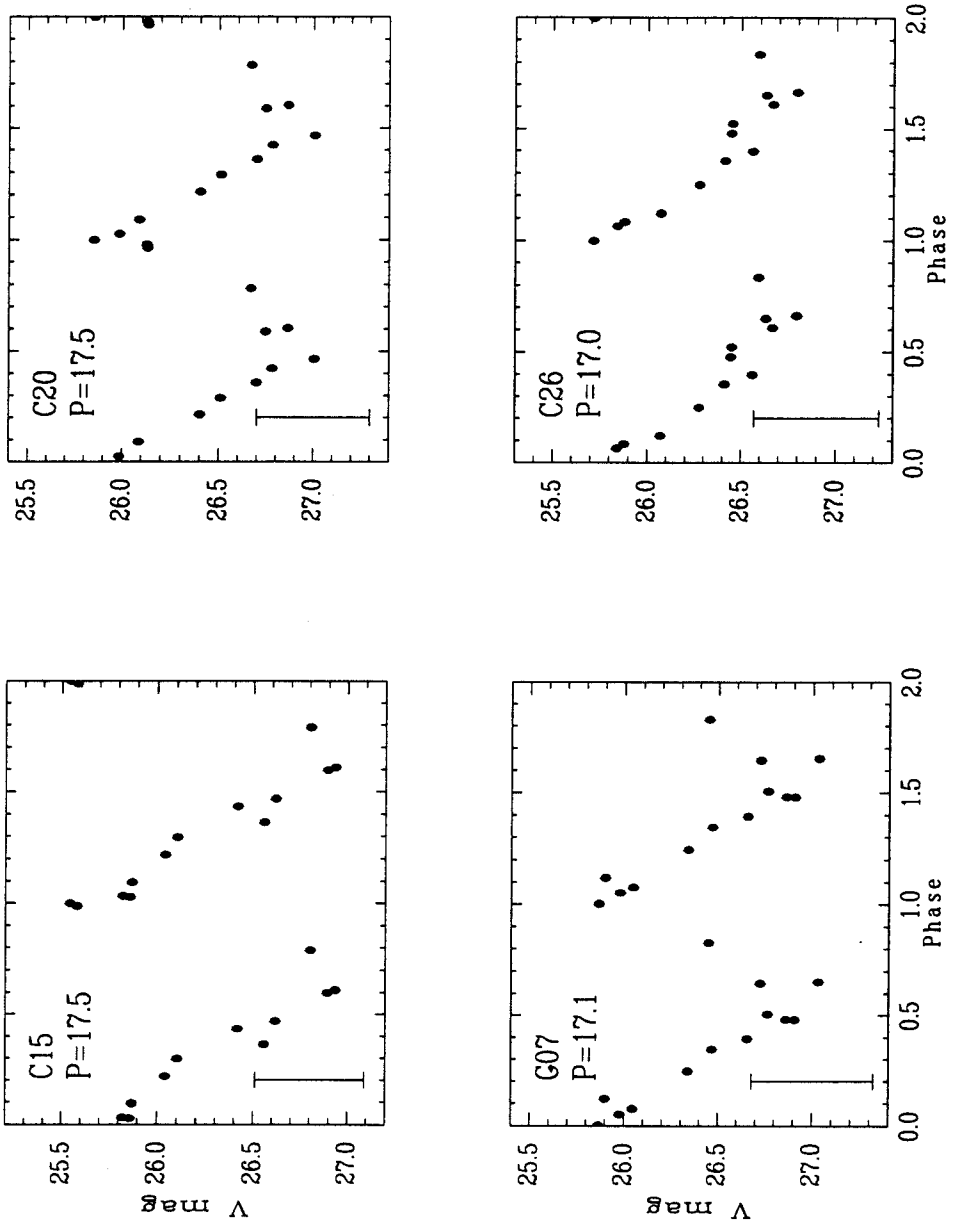
C15
P=17.5
C20
P=17.5
G07
P=17.1
C26
P=17.0
V mag
Phase
25.5
26.0
26.5
27.0
0.0
0.5
1.0
1.5
2.0

Figure 7f

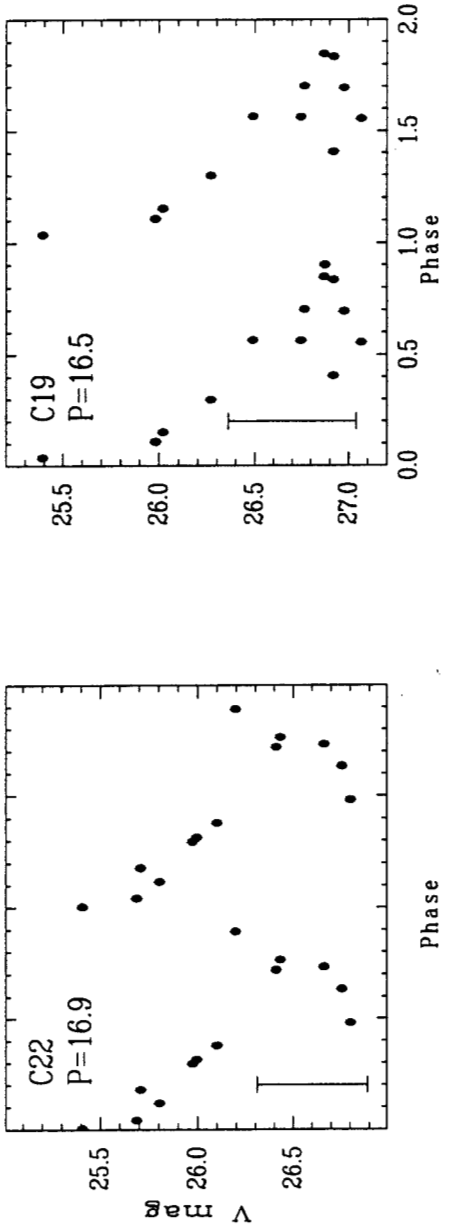

Figure 7g

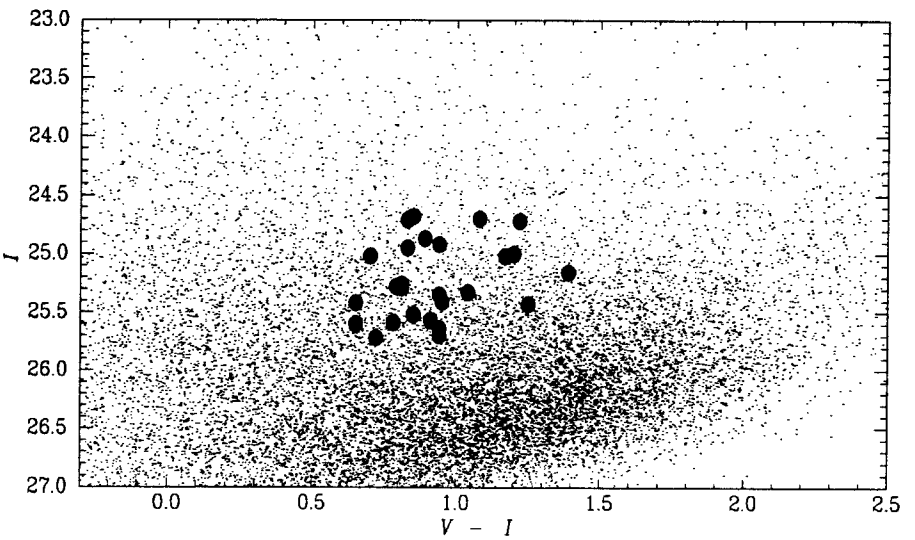

Figure 8

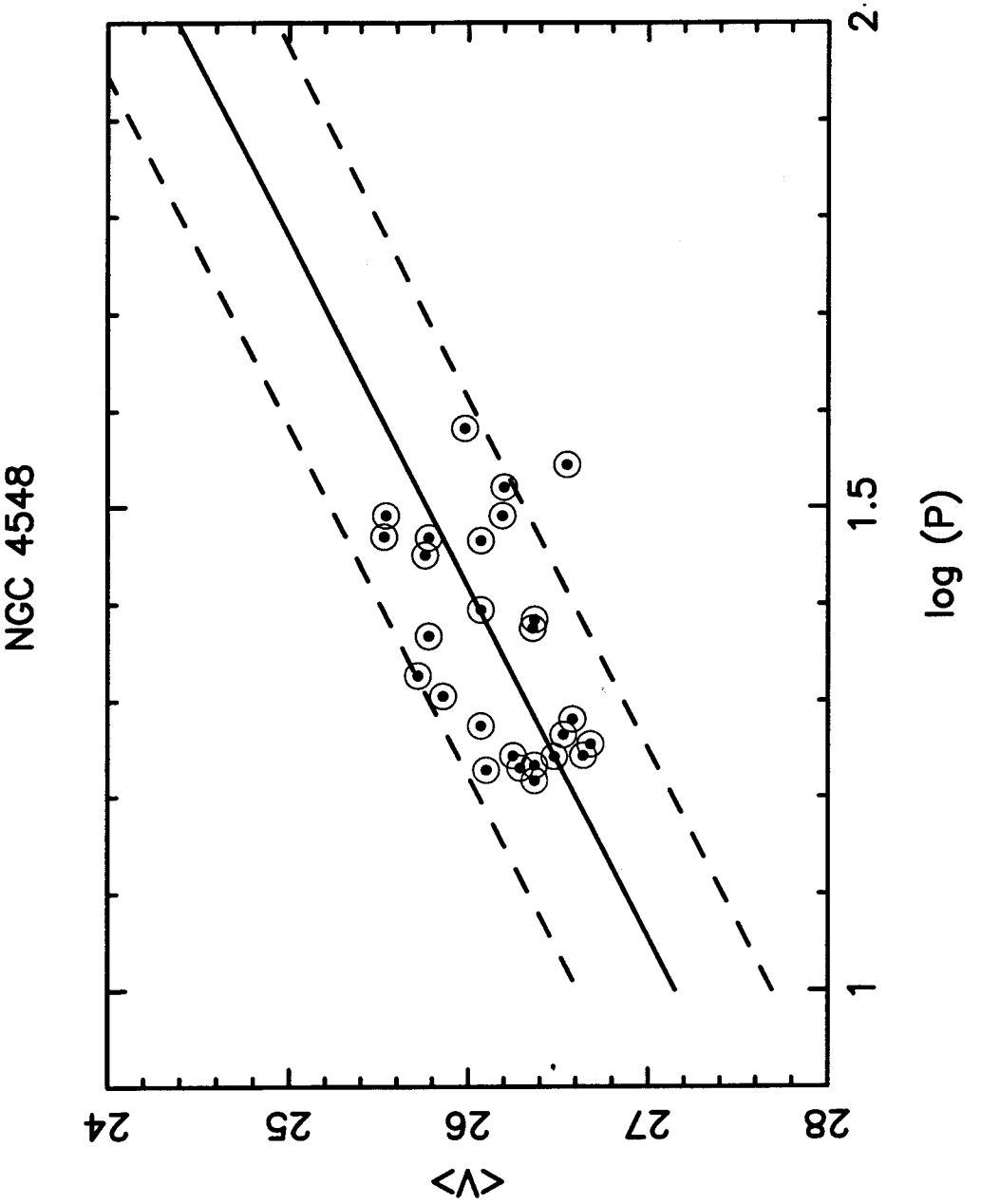

Figure 9

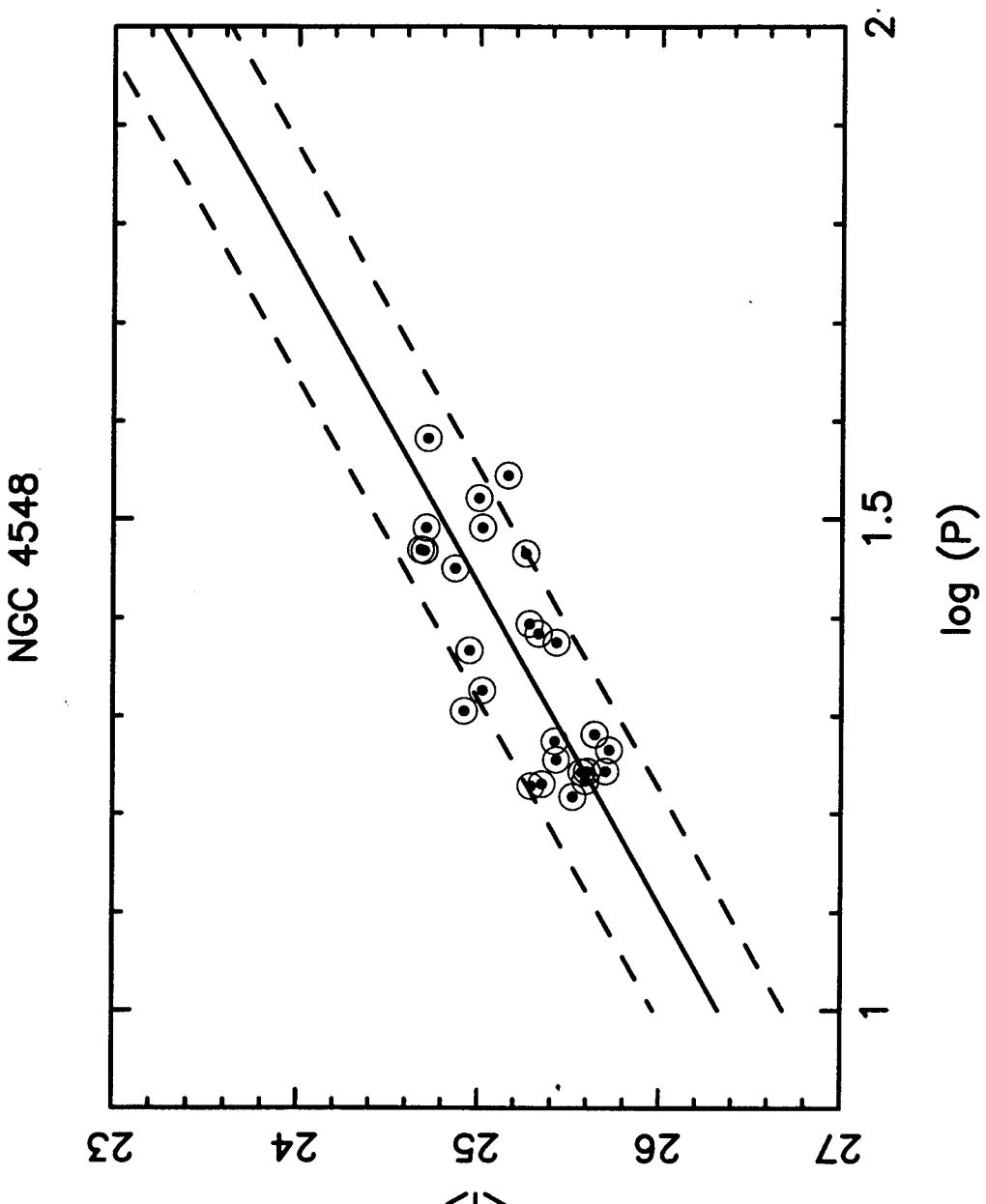

Figure 10